PROCESS IMPROVEMENTS FOR GAS BARRIER THIN FILMS DEPOSITED VIA LAYER-BY-LAYER ASSEMBLY

A Dissertation

by

DAVID AUSTIN HAGEN

Submitted to the Office of Graduate and Professional Studies of
Texas A&M University
in partial fulfillment of the requirements for the degree of

DOCTOR OF PHILOSOPHY

Chair of Committee,	Jaime Grunlan
Committee Members,	Jodie Lutkenhaus
	Debjyoti Banerjee
	Karl Hartwig
Head of Department,	Andreas Polycarpou

May 2015

Major Subject: Mechanical Engineering

ABSTRACT

Thin layers of aluminum have provided good oxygen barrier for food packaging for many years, but aluminum coatings can easily crack, are completely opaque, and are not environmentally friendly. One gas barrier solution for food, to flexible electronics, and pressurized bladders is to create polymer nanocomposite thin-films using layer-by-layer (LbL) assembly. These non-metal, water-based thin films contain a tortuous path through which a gas molecule must navigate. The work in this dissertation focuses on improving the process of creating these thin films to optimize their performance and achieve lower transmission rates with fewer layers.

Excellent gas barrier was achieved in a layer-by-layer thin film with fewer layers by optimizing deposition time of cationic polyethylenimine (PEI) and anionic poly(acrylic acid) [PAA]. Substantial deposition occurs with short deposition times for the first four PEI/PAA bilayers, while thicker deposition occurs with longer deposition times beyond 4 bilayers. Eight bilayers (650 nm) were required to achieve an undetectable oxygen transmission rate (<0.005 $cm^3/(m^2 \cdot day)$) using 1 min deposition steps, but this barrier was obtained with only 6 BL (552 nm) using 1s deposition of the first four bilayers, reducing total deposition time by 73%.

Polymer–clay bilayer films show good oxygen barrier properties due to a nanobrick wall structure consisting of clay nanoplatelets within polymeric mortar. Super oxygen barrier trilayer thin films have been deposited using two successive anionic layers of montmorillonite (MMT) clay and polymer (PAA) following every cationic polymer

(PEI) layer during layer-by-layer assembly. It is shown here that adding an anionic polymer layer reduces free volume of the film by filling in gaps of the similarly charged clay layer, which increases the barrier performance by at least one order of magnitude.

Barrier improvement can also be achieved by reducing the pH of the clay suspension in the PEI/MMT system. The charge of the deposited PEI layer increases in the clay suspension environment as the pH decreases, attracting more clay. This enables a 5× improvement in the gas barrier for a 10 PEI/MMT bilayer thin film (85 nm) made with pH 4 MMT, relative to the same film made with pH 10 MMT (57 nm).

DEDICATION

I would like to dedicate this dissertation to my grandparents, Dr. Jack and Sue Taylor, and parents, Drs. Michael and Barbara Hagen, for instilling in me the drive to accomplish great things to benefit my family and to accomplish God's work. You have provided the support and encouragement I needed to succeed at every level of my education.

ACKNOWLEDGEMENTS

I would like to thank my committee chair, Dr. Jaime Grunlan for his guidance and providing a means of financial support throughout the course of this research. I would like to thank Dr. Jodie Lutkenhaus, Dr. Debjyoti Banerjee, and Dr. Karl Hartwig for their time to serve on my committee and for their thoughtful insight given during my preliminary examination. I would also like to give special thanks Dr. Oren Regev (Ben-Gurion University of the Negev) for his teaching, especially on how to understand and proficiently operate a transmission electron microscope.

Thanks also go to the faculty and staff for making my time at Texas A&M University enjoyable and productive, including E. Ann Ellis, Rick Littleton, and Dr. Hansoo Kim at the Microscopy Imaging Center, Dr. Wilson Serem at the Materials Characterization Facility, Mitch Wittneben, Nicole Latham, Gina Gressettt, Crystal Morris, Isabel Cantu, and Holley Toschlog in the Mechanical Engineering Department. Thanks also to Eddy Garcia-Meitin at The Dow Chemical Company for his training to section thin films for observation under TEM.

I would like to thank all the present and former members of the polymer nanocomposites lab that I've had the pleasure to work with for their support and assistance, particularly Dr. Morgan Priolo, Bart Stevens, Fangming Xiang, Ping Tzeng, Kevin Holder, Blake Teipel, Dr. Galina Laufer, Morgan Plummer, Tyler Guin, Dr. Chungyeon Cho, Dr. Chungyeon Cho, Merid Haile, Yixuan Song, and Dr. Debrata Patra for their help in learning characterization methods, understanding the fundamentals of our work, and for

their friendship during the past three and a half years. Thanks also to the undergraduate assistants who helped me produce much of the data presented in this dissertation: Lauren Saucier, Brendan Foster, Chadley Box, Stephen Greenlee, and Aaron Milhorn.

I would like to thank my fiancé, Dr. Amanda Cain, for her encouragement, trust, faithfulness, and desire to seek the Lord in everything.

I would like to thank my former professors at Baylor University, Professor Emeritus Dr. Walter Bradley, Dr. David Jack, and Dr. Adam Ecklund for encouraging me to excel in my academic pursuits, to always be inquisitive, and to serve others. Thanks to my former internship managers Dr. Elisa Teipel and Bruce Golden for providing me opportunities to develop as an engineer. Thanks to Ed Braeuer, my high school physics teacher, for skillfully and creatively making our physics class the highlight of the school day and for sparking my interest in science and engineering. R.I.P. Coach Braeuer.

I would like to thank my siblings, Michael, Jon, Michelle, Tim, Jess, and Austin for pushing me to succeed in every realm of life and for all setting such high standards that challenged me. Thanks to my grandparents, Harry and Jean Hagen, for setting such good examples of how to work hard and enjoy family.

I would like to thank my friends at New Life Baptist Church, especially Nathan Forbes and Matt Kirby, for encouraging me through the difficult work of graduate school and helping me to keep a proper perspective of the value of a Ph.D.

I would like to thank God, for "every good and perfect gift is from above," (James 1:17) and "everyone who calls on the name of the Lord will be saved." (Romans 10:13)

NOMENCLATURE

AFM	Atomic Force Microscopy
ASTM	American Society for Testing and Materials
BL	Bilayer
CVD	Chemical Vapor Deposition
LbL	Layer-by-Layer
MMT	Montmorillonite
OTR	Oxygen Transmission Rate
PAA	Poly(acrylic acid)
PEI	Branched Polyethylenimine
PET	Poly(ethylene terephthalate)
PNC	Polymer Nanocomposites
PVD	Physical Vapor Depositoin
QCM	Quartz Crystal Microbalance
QL	Quadlayer
TEM	Transmission Electron Microscopy
TGA	Thermogravimetric Analysis
TL	Trilayer
UV-Vis	Ultraviolet-Visible Light Spectroscopy
VMT	Vermiculite
XRD	X-Ray Diffraction

TABLE OF CONTENTS

Page

LIST OF FIGURES

Page

LIST OF TABLES

Page

CHAPTER I

INTRODUCTION

1.1 Background

There is significant interest in transparent, flexible thin films that exhibit good oxygen barrier for applications such as food packaging, flexible electronics, and pressurized bladders.[1-3] There are potential benefits of using lighter weight gas barrier films in various pressurized systems, such as a decreasing a tire's rolling resistance or reducing aerostat's helium consumption. Flexible electronic displays require high gas barrier to protect the underlying components from photo-oxidative degradation. When, applied as a barrier layer, metalized films have been used to impart high oxygen and moisture barrier to polymeric substrates, but have a tendency to crack, are not recyclable, and are opaque.[1] These shortcomings are avoided with layer-by-layer (LbL) thin films. Despite its drawbacks, 1.7 million tons of aluminum were used for packaging in the US in 2005, much of this in metalized films.[4] Other barrier films have been developed, but each have significant limitations. SiO_x and Al_xO_y films exhibit good gas barrier, but they have a tendency to crack upon flexing and are deposited with a complex vapor deposition process that requires a vacuum environment.[5-6] Using clay as a filler in bulk polymer composites to improve the oxygen barrier has long been studied, but poor exfoliation, limited orientation, and restricted loading hinders barrier improvement.[7-9]

Thin film nanocomposites constructed using layer-by-layer (LbL) assembly are a good alternative to inorganic layers due to their tailorability, robustness, and simple

processing.[10] In addition to being excellent gas barriers,[11-16] these films have also been prepared for pharmaceutical,[17-19] superhydrophobic,[20-21] antimicrobial,[22] anti-flammable,[23-24] and electrically conductive[25-26] applications. This wide range of properties is made possible by the large variety of components that can be employed in LbL assembly: polymers,[27] nanoparticles,[28] quantum dots,[29] and biological molecules.[30] Beyond the constituents used, the properties of the composite films can be further tuned by varying molecular weight,[31-33] deposition time,[33-35] pH,[36-38] concentration,[39-40] ionic strength,[40-42] and temperature.[42-43] Although there are endless options for constituents and parameters, constructing a thin film using the layer-by-layer process is as simple as dipping a charged substrate into an oppositely charged solution, rinsing any excess material off the substrate, and repeating in an oppositely charged solution (followed by a second rinse), shown schematically in Figure 1, to produce a single bilayer. The beauty of the layer-by-layer process is its simplicity, which allows for the construction of an endless number of composite systems without the need for complex processing.

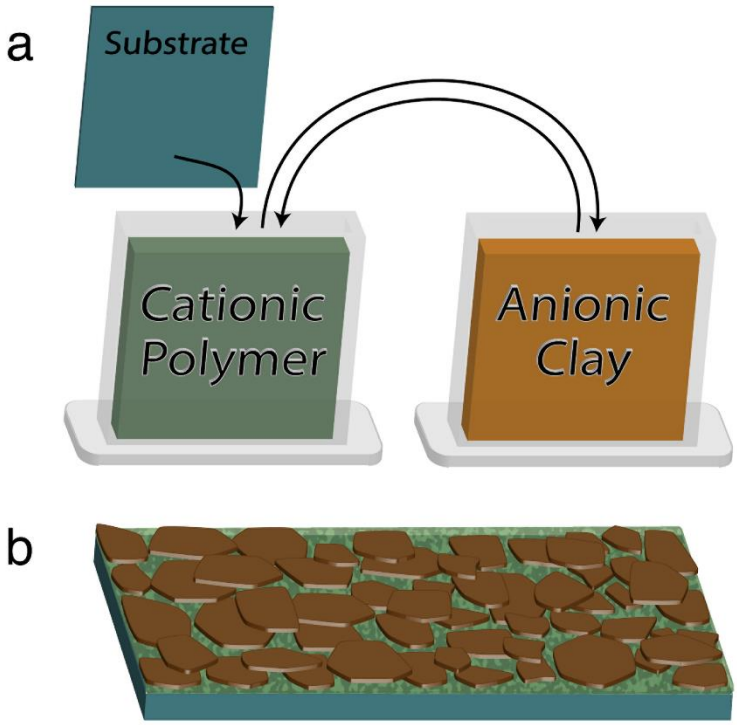

Figure 1. (a) Schematic the LbL deposition using the dipping method. (b) Simplified molecular conception of the first bilayer of a polymer/nanoparticle system being deposited onto a positively charged substrate.

The LbL process has been used to create very good gas barriers using bilayer (BL) and quadlayer (QL) systems that utilize impermeable nanoplatelets (e.g., clay and graphene oxide), each on the order of 1 nm thickness with aspect ratios up to several thousand, to create an extremely tortuous pathway for diffusion of gas molecules.[11-16] The water-based nature of the layer-by-layer process allows for highly exfoliated and oriented clay platelets to be deposited every cycle, generating a nanobrick wall structure. This structure provides superior properties over bulk composites, where aggregation and random orientation lead to increased opacity and greater gas permeability.[13]

The primary focus of this dissertation work was to develop techniques to make LbL thin films that are more effective at blocking oxygen with fewer deposition steps and less processing time. These process improvements will assist the adoption of LbL into commercial use. Reducing deposition steps and processing time require understanding the structure-property relationships of these thin films. Changing parameters that alter the fundamental interactions of the constituent materials provides optimum deposition and ordering of the multilayer thin film for better gas barrier properties.

1.2 Outline of Dissertation

Chapter II gives an overview of common barrier films that include polymer films and inorganic thin films (and the processes used to create them). Compatibility concerns and common methods for creating bulk composites with nanofillers are reviewed, including improvements made to gas barrier properties of these bulk composites. Finally, an introduction to layer-by-layer assembly is provided, with a review of the state of the art in gas barrier that led to the present work.

Chapter III investigates the influence of deposition time on thickness and properties of a layer-by-layer thin film constructed with polyethylenimine (PEI) and poly(acrylic acid) [PAA]. Excellent gas barrier was achieved with fewer layers by optimizing deposition time. Substantial initial deposition occurs with short deposition times for the first four bilayers, while thicker deposition occurs with longer deposition times beyond 4 bilayers.

Chapter IV examines the influence of employing successive negatively-charged layers of montmorillonite (MMT) clay and PAA after every positive PEI layer. Polymer-

clay bilayer films show good oxygen barrier due to a nanobrick wall structure consisting of clay nanoplatelets within polymeric mortar. It is shown here that adding an anionic polymer layer reduces free volume of the film by filling in gaps of the similarly charged clay layer and increases the barrier performance over the bilayer configuration by at least one order of magnitude.

Chapter V explores the influence of pH on the deposition of MMT in a PEI/MMT system. Reducing clay pH was found to increase the charge of the deposited PEI when introduced to the clay suspension environment, which causes more clay to be deposited. At pH 4, MMT platelets deposit with near perfect ordering, observed with TEM, enabling a 5× improvement in gas barrier for a 10 PEI/MMT bilayer thin film (85 nm) relative to the same film made with pH 10 MMT. This improved gas barrier approaches that achieved with much higher aspect ratio vermiculite clay. In essence, lower pH is generating higher effective aspect ratio for MMT due to greater induced surface charge in PEI layers that causes heavier clay deposition.

Chapter VI provides conclusions for the work in Chapters II-V and outlines suggested topics for future research based on this dissertation. This dissertation investigates the effects of deposition time, successive anionic depositions, and altering the pH of clay suspensions. These different aspects of improving gas barrier thin films can be paired and also be used to improve the gas barrier of quadlayer systems. Specific directions for incorporating these ideas with preliminary results are included. Demonstrating the ability of LbL to be scaled up to a continuous process is crucial for introducing this technology to commercial applications. Preliminary results from films constructed using a continuous dipping process have been obtained using a lab scale coater created in-house.

CHAPTER II

LITERATURE REVIEW

2.1 Gas Barrier Films

Polymers are widely used for food packaging due to their low cost, flexibility, desirable thermal and mechanical properties.[44] Some polymers have satisfactory barrier properties for lower sensitivity food products, but most are used as a substrate for a higher barrier layer that meets the requirements of more sensitive food, organic electronics, and vacuum insulating panels (VIP). The oxygen and moisture barrier requirements for these applications are shown in Figure 2.[45] Aluminized plastic film is the most widely used barrier for food packaging due to its low cost and the maturity of the technology. There has been a general push to move away from aluminum coated films because of the desire for package transparency, and environmental (and health) concerns.[46-47] Packaging has been constructed from polymer blends and as multilaminate systems in an effort to reduce cost, improve transparency, reduce moisture sensitivity, and increase shelf life.

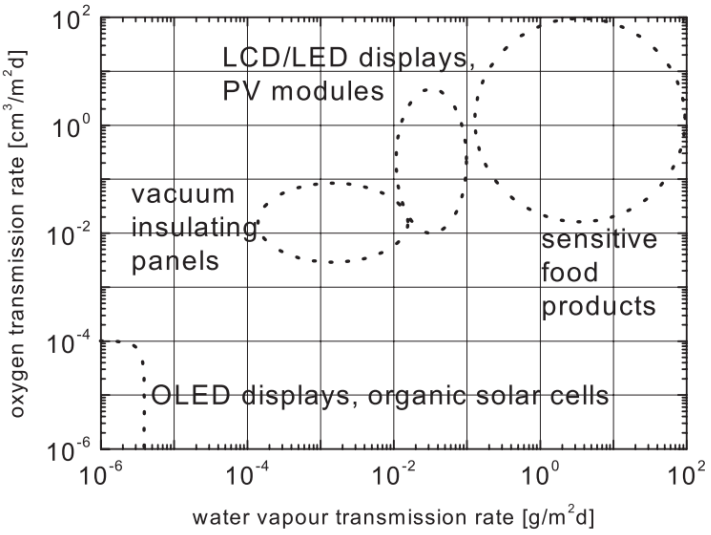

Figure 2. Barrier requirements for various applications.[45]

2.1.1 Polymer Barriers

Most polymers with very low permeability to oxygen are expensive and/or moisture sensitive. In order to reduce the amount of expensive barrier polymers, laminated films (via co-extrusion or co-injection) can be used to provide a continuous laminar structure to block out oxygen. Polymer blends can also be used, which often allows for a less expensive manufacturing process, but do not provide as significant an improvement in barrier properties as lamination does for the same loading, shown in Figure 3. Lamination and polymer blends are also used to reduce moisture sensitivity of high oxygen barrier polymers (e.g., EVOH within PE).[46] The permeabilities of many commonly used polymers are summarized in Table 1. Most of the moisture-sensitive polymers have been tested at 0% RH and are typically laminated with a commodity polymer that acts as a good moisture barrier (e.g. PE or PP) to protect them from water.

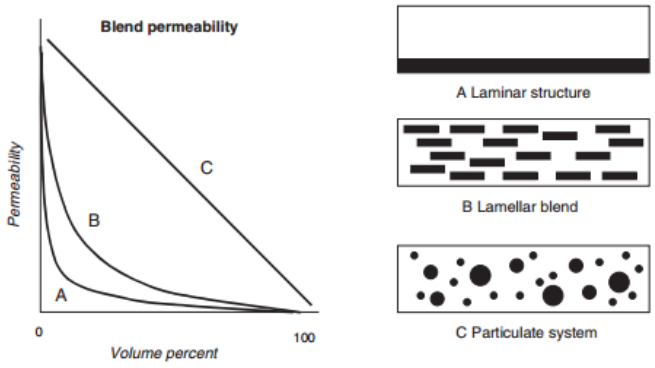

Figure 3. Schematic showing how permeability of a blend depends on morphology.[46]

Table 1. Permeability of common polymers used as packaging materials at 23°C.[46]

Polymer (abbreviation)	Oxygen permeability ($cm^3 \cdot mm/m^2 \cdot day \cdot atm$)	
Ethylene vinyl alcohol (EVOH)	0.01–0.1	0% RH
Polyethylene (PE)	50-200	50% RH
Poly(ethylene-terephthalate) (PET)	10–50	50% RH
Poly(lactic acid)[48] (PLA)	184	0% RH
Poly(vinyl chloride) (PVC)	20–80	50% RH
Polyamide (PA)	1–10	0% RH
Polypropylene (PP)	494–987	50% RH
Polystyrene (PS)	987–1481	50% RH
Polyvinylalcohol (PVOH)	0.2	0% RH
Polyvinylidene chloride (PVDC)	0.1–3	50% RH

2.1.2 Inorganic Barrier Thin Films

2.1.2.1 Physical Vapor Deposition of Aluminum

Films deposited with physical vapor deposition (PVD) have a wide range of applications including integrated circuits, medical instruments, pharmaceuticals, balloons, and mirrors. The primary methods of PVD are vacuum deposition, sputter deposition, arc vapor deposition, and ion plating, as shown Figure 4.[49] Vacuum deposition, also referred to as vacuum evaporation or metallization, is the primary method used for food packaging applications (first performed in the 1920's) and has been widely used since the 1970's.[50-51]

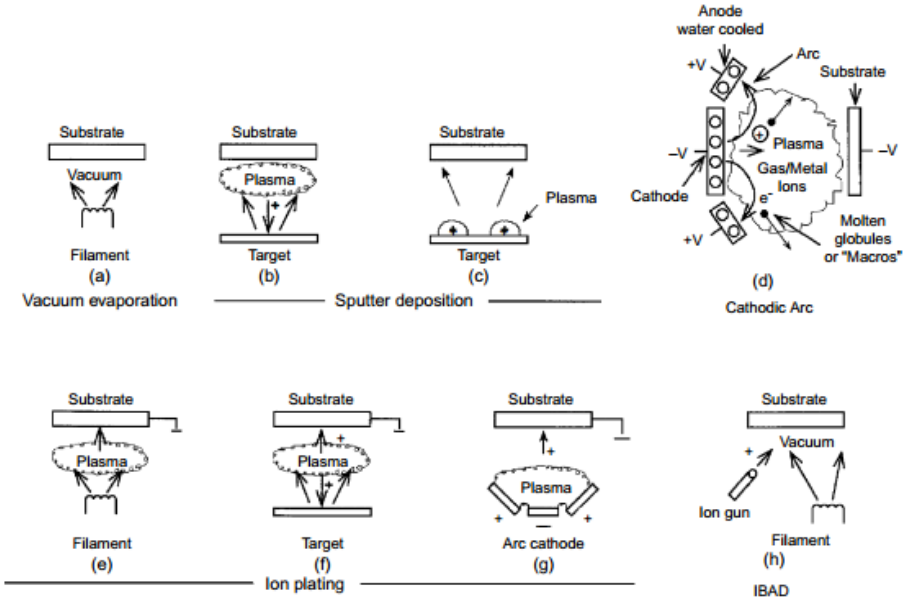

Figure 4. PVD processing techniques (a) vacuum evaporation, (b) and (c) sputter deposition in a plasma environment, (d) sputter deposition in a vacuum, (e), (f), and (g) ion plating in an plasma environment, and (h) ion beam-assisted deposition (IBAD).[49]

The material to be deposited (e.g. aluminum) is heated, causing it to vaporize and deposit onto the surface of the substrate, such as a moving plastic film in a roll-to-roll process. The metal is ejected from the molten surface and will collide with every surface within the chamber that has a direct line of sight with the reservoir of material. This process can cause pinholes if there are any particles present due to no material being deposited in the "shadow" of the particle, Figure 5. Also, a large pinhole can occur if that particle desorbs from the surface. For rough surfaces, the same shadowing effect can cause pinholes to form, also shown in Figure 5. The coating material can be heated in a number of ways, but focused e-beams and resistive heating are the most common for temperatures above and below 1500°C, respectively. The film is usually positioned relatively far away from the film as to not thermally degrade the film. A high vacuum (10^{-7}-10^{-10} Torr) is necessary to provide a sufficient mean free path to avoid collisions between the atoms from the thermal vaporization source and residual gas molecules near the substrate and to avoid film contamination.[52]

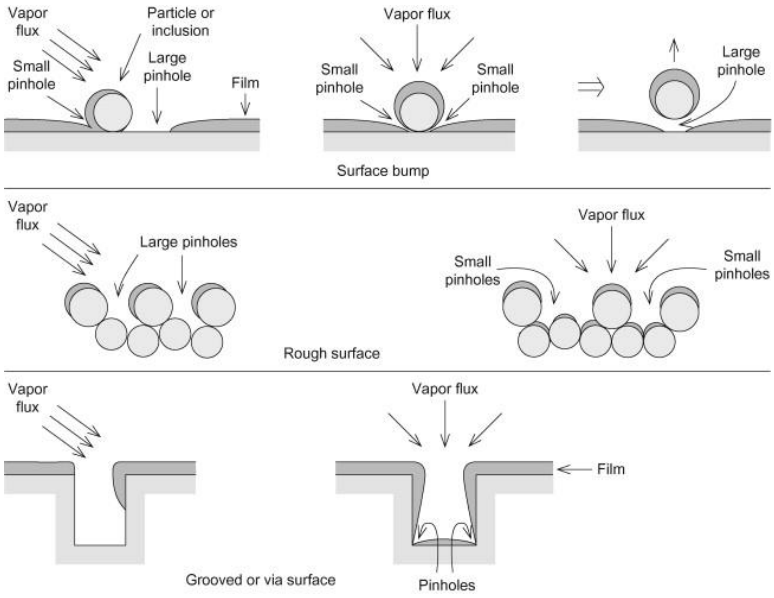

Figure 5. Geometrical Shadowing of the deposition flux by a particle on the surface and by surface features.[50]

Copper, silver, and stainless steel can also be deposited with PVD with a deposition rate of 1-10 nm/s and total thicknesses in the nm to μm range. All of these metals have a tendency to crack, which leads to a degradation of barrier properties as the package is handled. The composites are not recyclable, which adds waste to landfills. Opacity is a another drawback of these films, which limits their use in photovoltaics or screen encapsulation and leaves no way to view contents when used for food packaging.[1] The inability to microwave further limits the use of metallized film in food packaging.

2.1.2.2 Thin Oxide Films

Oxide films exhibit good gas barrier, but they have a tendency to crack upon flexing and are deposited with a vapor deposition process requiring a vacuum environment, much like metallization.[49, 53] Because these materials have high melting

temperatures, it can be difficult to produce coatings on polymer substrates with low thermal stability, especially at a high enough rate to become economical. While they are normally deposited using chemical vapor deposition (CVD), some (e.g. silicon oxide) can also be deposited with the PVD method discussed previously. CVD uses chemical precursor vapors that are reduced or decomposed at high temperatures, with the products either depositing onto or chemically reacting with the substrate. The deposited material can also form other compounds, such as nitrides and oxides, by reacting with gasses present in the deposition chamber. The reaction does not come to completion due to a constant influx and mixing of gas, so CVD normally involves an exhaust of unused precursor vapors and volatile byproducts, as shown schematically in Figure 6. Silicon nitride (SiN_x) can be deposited using catalytic chemical vapor deposition (Cat-CVD), or hotwire CVD (in environments below 100°C) by using a heated catalyzer.[54-55] A gas mixture of N_2H_4, N_2, and SiH_4 is introduced into the chamber that contains a 2% thoriated-tungsten (TH-H) wire used to decompose hydrogen, shown schematically in Figure 7.

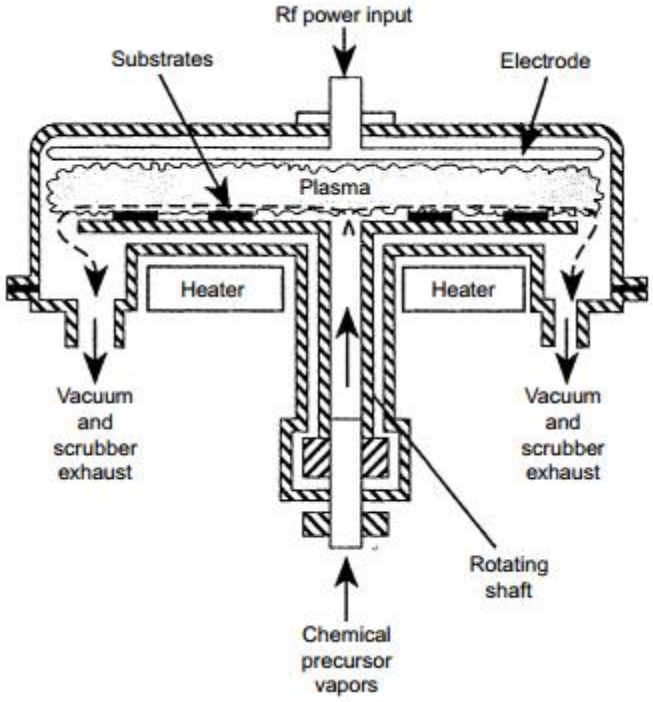

Figure 6. Schematic diagram of a Parallel Plate Plasma-Enhanced Chemical Vapor Deposition (PECVD) Reactor.[50]

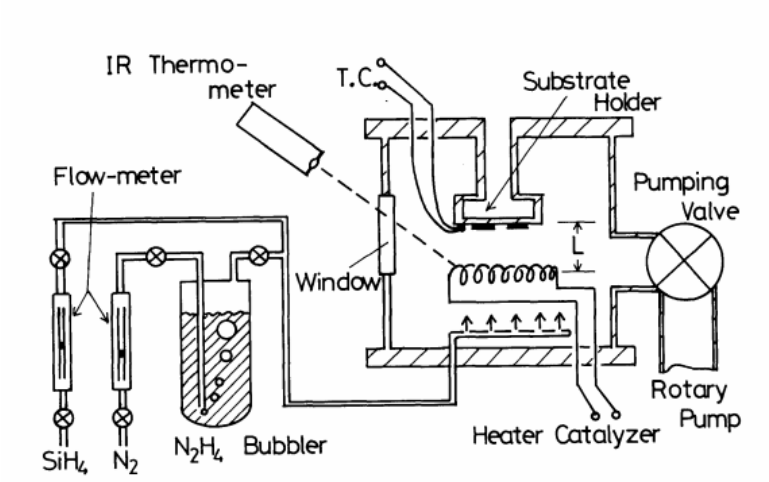

Figure 7. Schematic diagram of Cat-CVD deposition apparatus.[55]

Atomic layer deposition (ALD) is another thin film deposition method use for creating barrier thin films that is similar to CVD in that precursor vapors are used to deposit material on a surface. In ALD, the materials are deposited one at a time. The self-limiting reactions create a conformal coating with a highly ordered structure.[56] Recently, Al_xO_y has been deposited onto oriented polypropylene (OPP) using reactive PVD and exhibits an excellent oxygen permeability of 1.83×10^{-19} $cm^3 \cdot cm/(cm^2 \cdot s \cdot Pa)$, but requires lamination with a protective layer for packaging applications.[57] SiO_x films (13-70 nm thick) on PET have been examined for gas barrier properties and it was found that the permeability is much higher than bulk silica glass due to permeation through the lattice structure, nano-defects, and macro-defects (pinholes) in the oxide layer.[58] Even so, the permeability of SiO_x films is slightly lower than Al_xO_y at 1.14×10^{-20} $cm^3 \cdot cm/cm^2 \cdot s \cdot Pa$.[59]

2.2 Traditional Polymer Nanocomposites

Polymer nanocomposites (PNC), for the purpose of this review, will be defined as a system containing polymer and a second material with at least one dimension in the nanometer range, which could also be a polymer. PNCs in bulk have been studied extensively to stiffness, strength, toughness, thermal stability, electrical conductivity, electrical insulation, and gas barrier properties.[60-66] In order to impart good barrier behavior, along with many other properties, particles must be well dispersed and have good interfacial adhesion with the matrix.

2.2.1 Preparation Techniques of Traditional Nanocomposites

Good interfacial adhesion is obtained through proper compatibility between the particles and the matrix; this can come from surface treatment or proper selection of material for the surface of nanoparticles. Surface treatment has been used to ensure compatibility with matrix and provide good dispersion for many different inorganic particles. Chemical treatments that react with O-H species present on the surface of the nanoparticles have been performed on nanoparticles with the following various coupling agents including organosilanes, metal alkoxides, epoxides, and isocyanates.[67] Silane coupling agents occupy the majority of academic focus for chemical treatments of nanoparticles.[68-75] Silane coupling agents are normally in the form $RSiX_3$, where R is an organofunctional group (such as vinyl, amino, methacryloxy, and epoxy groups) and X represents a halide, alkoxide, acrylate, amino or alkyl group.[67] The X groups form covalent bonds with the surface O-H groups of the nanoparticle and the attachment of the functional group effectively links the particles to the matrix. Nanoparticles, such as TiO_2, Al_2O_3,

Fe_3O_4, SiO_2, and ZnO, treated with silane coupling agents have been shown to have better dispersion in organic solvents and polymer matrices due to a lower affinity between particles and increased affinity between polymer and matrix.[76-77]

Grafting of synthetic polymers is another surface treatment used to improve adhesion and dispersion of nanocomposites. Grafting can be done in two methods, "Grafting from" and "Grafting to" shown schematically in Figure 8. Grafting from the nanoparticle involves attaching an anchor layer onto the surface of the nanoparticle followed by polymerization of monomer that is introduced, which shows a higher percentage of successful grafts. Grafting to is done simply by introducing an end-functionalized polymer that will react to the nanoparticle surface.[78] Adsorption of polymeric dispersants is one of the simplest methods to improve dispersion if adhesion is not an issue. Anionic or cationic polymer dispersants are used to disperse hydrophilic nanoparticles (which would normally aggregate in a polymer matrix).[79]

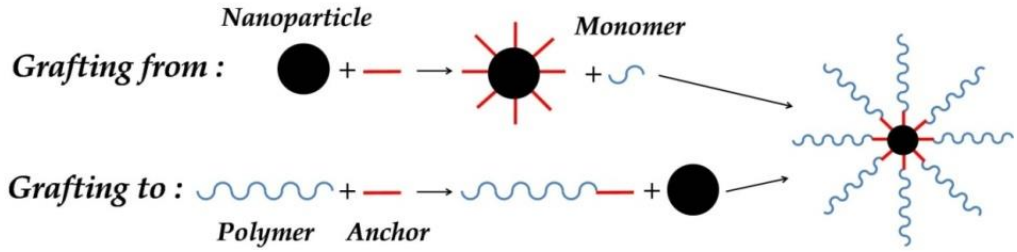

Figure 8. Presentation of grafting from and grafting to methods.[80]

The proper preparation technique is very important when trying to ensure a consistently well dispersed composite. Melt-processing (melt blending) is the simplest method, but it does not always provide a well dispersed composite due to the formation of agglomerates. Solution blending uses a solvent to dissolve or suspend the polymer and nanoparticles to allow high mobility between the two phases for good dispersion.[81] The solution is then cast and allowed to dry, leaving the polymer composite behind as the solvent evaporates. The use of the solvent and its recovery can add significant cost to this fabrication method. In-situ polymerization involves the formation of nanoparticles within the polymer matrix through incorporation of nanoparticle precursors, usually gas or liquid, into the matrix. Chemical reductions, photoreductions, and thermal decompositions have all been used for the insitue fabrication of nanoparticles.[82] Taking this method one step further, it is possible to form both the polymeric matrix and the nanoparticles by injecting the precursor of the nanoparticles into polymerisable monomer supply, and the polymer matrix can be created simultaneously during the generation of nanoparticles.[83] To ensure that naturally occurring MMT is well dispersed in a polymer matrix, clever methods have been used to create bulk nylon composites and multilayer thin films.

One of the most successful polymer-clay composites is the nylon 6-clay hybrid (NCH) developed by Kojima and team at Toyota. By using a 4.7 wt. % loading of montmorillonite (MMT) clay, they were able to significantly increase its mechanical properties.[84-85] MMT powder was mixed with hydrochloric acid (HCl) and ω-amino acid [$H_3N+(CH_2)n-1$ COOH, n = 2-12 and 18] in water where the ammonium ion of the ω-amino acid was exchanged with a sodium ion of MMT.[86] This swells the silicate layers

with ω-amino acid by "grafting to" the surface. The clay platelets were further swollen in the presence of caprolactam. Ion-exchanged MMT powder, termed "n-montmorillonite," was obtained by freeze drying the solution. X-ray diffraction (XRD) was done on the different powders to calculate the basal spacing, explained in XRD section below. 12-aminolauric acid was chosen because it provides a significant increase in d-spacing of the MMT and is widely available, shown in Figure 9. The authors propose that the carboxylic acid tail of the 12-aminolauric acid hydrogen bonds with the -O- group on the clay surface.

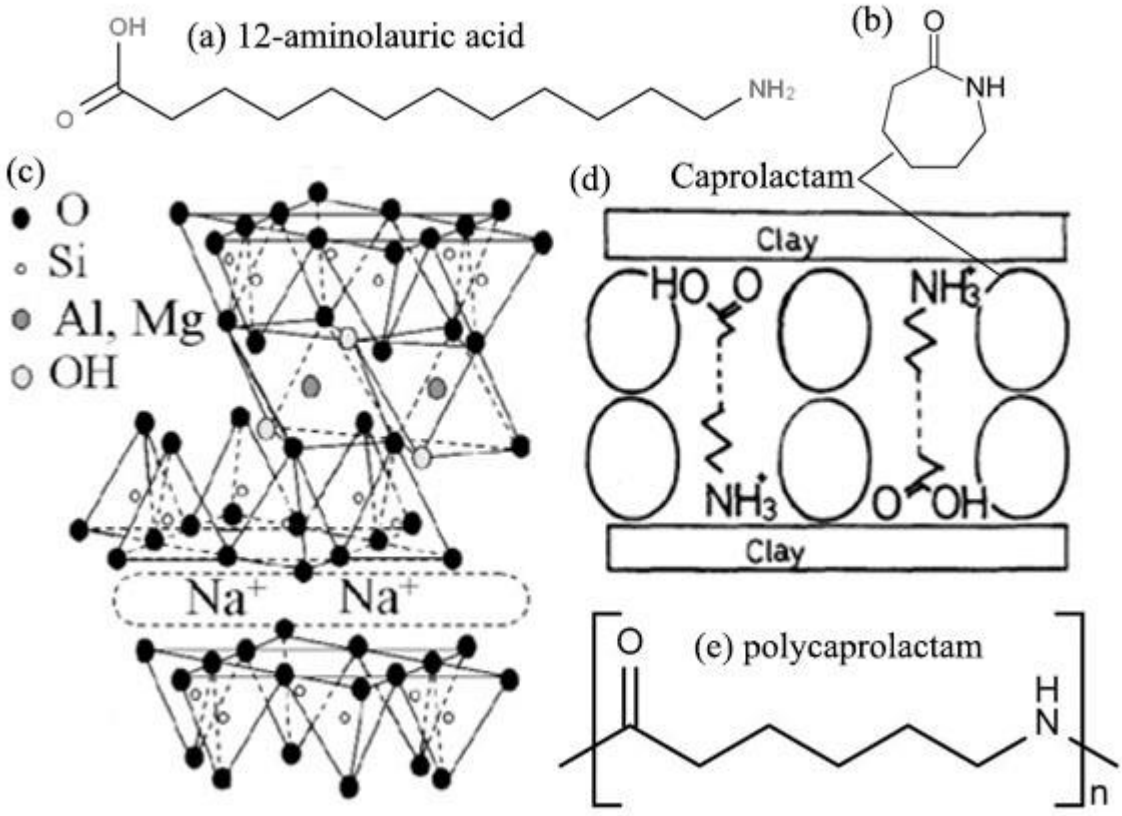

Figure 9. Illustrations of (a)12-aminolauric acid, (b) caprolactam, (c) sodium montmorillonite, (d) swollen montmorillonite, and (e) polycaprolactam (nylon 6)[86-87]

From this point, 12-montmorillonite and caprolactam were combined and heated above 250° to polymerize caprolactam within and around the expanded montmorillonite, keeping the MMT platelets well separated.[85] 6-aminocaproic acid was used in small amounts as a catalyst to increase the ring opening polymerization rate of caprolactam. This mixture of 12-montmorillonite and polycaprolactam was found to be suitable for injection molding at loadings up to 7 wt% clay. Figure 10(b) shows a TEM micrograph of the clay platelets which are oriented in the flow direction, dispersed, and exfoliated throughout.

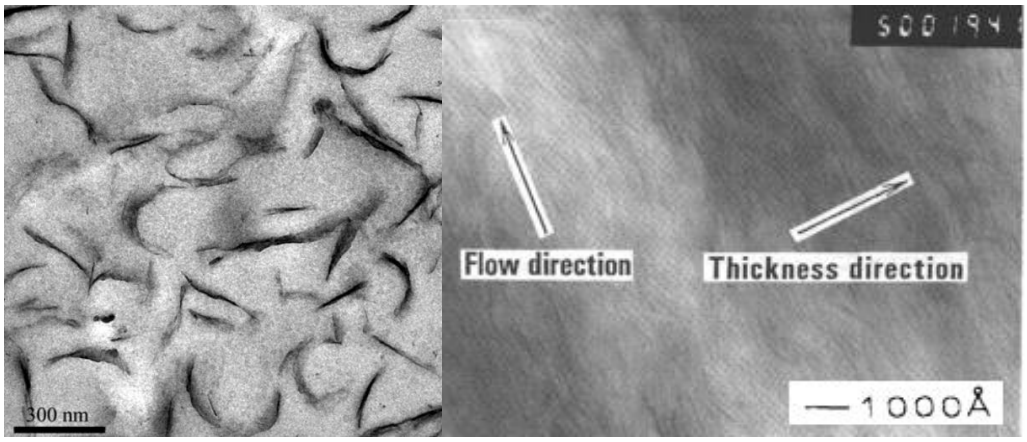

Figure 10. TEM micrographs of (a) 3.5 vol% MMT in epoxy with poor exfoliation and orientation and (b)Nylon 6 with 4.7 wt% MMT. [84, 88]

2.2.2 Gas Barrier of Traditional Composites

It has been theorized for many years that the inclusion of impermeable flakes in a polymer matrix would significantly reduce the overall permeability. This was originally proposed by Nielsen in 1967 and later expanded upon by Cussler.[89-91] Nielsen's rational was that by including particles within the matrix, the diffusion path of the molecule would be greatly increased. He defined a tortuosity (τ) factor of the system to be

$$\tau = 1 + \left(\frac{L}{2W}\right)\phi \tag{2.1}$$

where L is the length of the filler particle, W is its thickness, and ϕ is the filler volume fraction. As the aspect ratio (L/W) of the particles and the filler volume fraction increases, the tortuosity greatly increases. This model assumes platelets of the same size uniformly aligned perpendicular to the direction of gas permeation. The molecules are assumed to diffuse straight through the film until coming upon a platelet and then travel laterally until coming upon a slit (gap in platelet coverage) and immediately permeate through the slit, moving through the film in a staircase pattern, shown in Figure 11(a). The permeability of the composite (P_c) is

$$P_c = P_p\tau \tag{2.2}$$

where P_p is the permeability of the polymer. Equation 2.2 was derived for a very low loading of platelets ($\phi<<1$). Cussler improved upon this model with the idea that the oxygen molecule "wiggles" through the galleries between clay platelets as it diffuses through the composite. This model also attempts to account for the resistance of the molecule to permeate through the slits. Cussler's equation for relative permeability of the composite is:

$$\frac{P_p}{P_c} = 1 + \mu\alpha^2\left(\frac{\phi^2}{1-\phi}\right) \quad (2.3)$$

where μ is geometric factor based on the filler, α is the aspect ratio, *d/t* (*d* is the diameter of the flake and *t* is the thickness).[90]

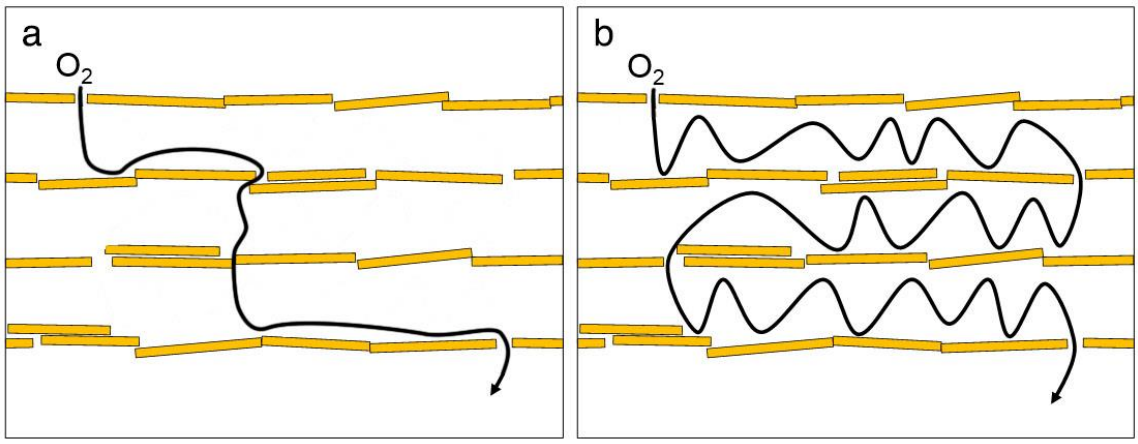

Figure 11. Schematic of (a) Nielsen's tortuosity model where Oxygen will diffuse through the first possible slit in the clay coverage and (b) Cussler's model that includes diffusion "wiggles" between clay layers. Adapted from[92]

Adding clay platelets to polymer matrices leads to a significant decrease in oxygen permeability, but there has been difficulty in attaining the level of oxygen barrier as predicted by Cussler's model due to the challenge of adequately exfoliating clay stacks and appropriately aligning platelets. Oxygen barrier improvement ranges from 2-20X improvement over unfilled polymer.[9, 88, 93-97] One specific epoxy/clay system exhibited an improvement of 3 orders of magnitude over the base epoxy. This composite was created by first carefully crafting a clay fabric via evaporating the water from a 5% clay solution

and impregnating it with epoxy.[98] In the absence of heroic processing measures, it is atypical to exceed a 10× improvement in oxygen barrier with bulk nanocomposites.

2.3 Layer-by-Layer Assembly

2.3.1 Introduction to Layer-by-Layer

The layer-by-layer deposition process began in 1966 at DuPont, when R. K. Iler discovered that positively and negatively-charged colloidal particles could be deposited onto one another alternately from suspensions, constructing a thin film on a charged surface.[99] It was correctly assumed that multilayers could be created in this manner using small particles, polyvalent ions, surfactants, and water-soluble polyelectrolytes. Using this method to deposit oppositely charged polyelectrolytes did not appear in literature until 1992, when Decher and colleagues used polystyrenesulfonate and polyvinylsulfate, (i.e., anionic polymers), and poly-4-vinylbenzyl-ammonium and polyallylamine, (i.e., cationic polymers).[100] They demonstrated that this process could be used to construct films to at least 100 BL, with an average bilayer thickness of 2.3 nm. Many other materials have since been used including many different synthetic and natural polymers, dendrimers, carbon nanotubes, graphene oxide, metals, metal oxides, various clays, quantum dots, ligands, nucleic acids, proteins, enzymes, viruses, and therapeutics.[22, 27-30, 101-103] Applications for LbL assembled thin films and include biomedical (tissue engineering, drug delivery, biosensors, anti-microbial),[104] electrochemical (energy storage and conversion),[105] superhydrophobic,[20-21] anti-flammable,[23-24] and films that react to light,[106] heat,[107] and pH[108] (in various ways).

Since Iler's and Decher's initial work, there has been significant development of LbL systems, but the basic premise of dip coating has remained the same: a charged substrate, flat or three dimensional, is submerged into a liquid containing a solution of oppositely charged polyelectrolyte. The substrate remains submerged between one second to tens of minutes.[35, 40, 109-113] There is typically rinsing after each deposited layer either by dipping into a container of purified water or via an active stream of rinse water. After rinsing, the film is often dried with filtered air. The rinse and dry steps are done for consistency in an academic setting, but are not necessary for every system. Removing these steps would further simplify the process, making it a very attractive method for industrial applications. Proof of concept for a large-scale continuous immersion process has been demonstrated on a simple homebuilt system,[114] and further improvements are described in Chapter VI. Two other methods that have been investigated for deposition of LbL systems are spray-assisted[115-118] and spin-assisted[29, 118-119] LbL deposition. Spraying provides a much different route for deposition, bringing the solution to the substrate instead of the substrate to the solution, as in a dip process (both shown in Figure 12). While spraying can easily coat a flat substrate, three dimensional substrates can become problematic if trying to coat conformally. Coating of nonwoven electrospun fiber scaffolds was controlled by altering the flowrate of the materials.[120] Increasing the flow rate created much fiber bridging, while lower flowrate allowed for a somewhat conformal coating of the outermost fibers. Spraying allows for a plateau of adsorption for each layer more quickly, but reaching this plateau is not necessary to construct a function film, also, throughout many variables tested by Izquierdo et. al., dipping always provided a thicker

film.[115] Spin coating can provide a more stratified film due to shear forces and solvent evaporation, which can both limit diffusion. This can lead to a smoother and thinner film than would be obtained with dip coating.[121] There are other variations to LbL deposition for specific purposes. Perfusion uses a dropwise addition of constituents onto a scaffold of dissolvable spheres that leaves behind a porous scaffold of thin film for tissue engineering.[122-123] Hydrodynamic-dip-coating is a method used to increase deposition rate by agitating the solution.[124] Inkjet printing assisted LbL allows selective deposition to a given area and allows for control by adjusting volume applied at the picoliter scale.[125]

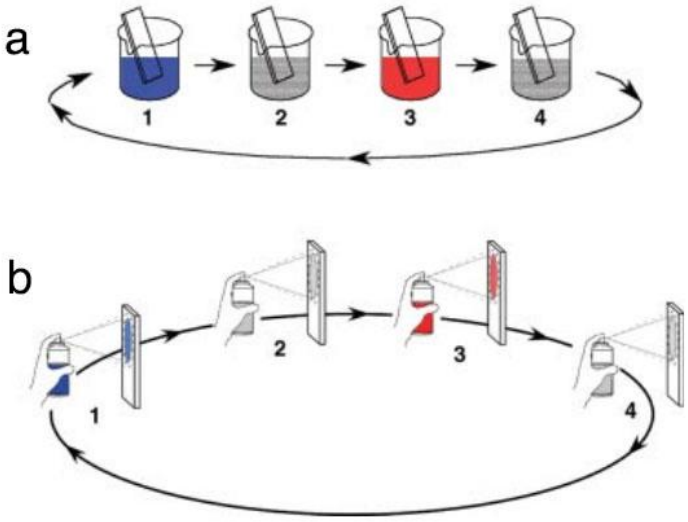

Figure 12. Schematic of the LbL deposition process using the (a) dipping and (b) spraying methods.[118]

LbL deposition has several advantages over other atomic assembly methods, such as Langmuir-Blodgett (LB), which require expensive, specialized instrumentation, long construction times, and the need for amphiphilic molecules.[101] LbL films can be produced on a lab scale under ambient conditions by simply hand-dipping a substrate into solution (scale up requires only simple machinery), can be deposited in a matter of seconds, and allows a wide range of materials choices. In addition to electrostatic interactions, LbL thin films can be constructed using hydrogen bonding and hydrophilic interactions.[27, 101] LbL thin films also tend to be much more stable than LB and self-assembled monolayers (SAM). These techniques often require special surface chemistries to allow formation of monolayers and specific compounds are needed to allow formation of monolayers (e.g. thiols and silanes).[126] Layer-by-layer assembly is also much safer and simpler than the PVD and CVD processes described in Section 2.1.2. High temperatures, high vacuum, and a high sensitivity to contamination add cost and complexity to commercial vapor deposition processes, none of which apply to LbL deposition.

Persuading clay, or other hydrophilic particles, to readily go into a polymer matrix with good dispersion and interfacial adhesion requires extensive modification and processing that add considerable cost and time to the process. Even a well dispersed clay-based PNC system produced via melt mixing has not provided more than an order of magnitude improvement in oxygen barrier.[46, 127-131] Layer-by-layer constructed thin films have no compatibility issues between clay and polymer because of the electrostatic attractions between them.[132]

2.3.2 Gas Barrier of Layer-by-Layer Thin Films

The first LbL thin film reported to have good oxygen barrier was constructed by Kotov and colleagues in 1998.[132] With 50 bilayers of poly(dialyldimethylammonium chloride) (PDDA)/MMT (200 nm thick) on 25 μm PET, the oxygen transmission rate was reduced from 80 to 10 $cm^3/(m^2 \cdot day \cdot atm)$, but the moisture transmission rate was virtually unchanged. The PEI/MMT nanobrick wall system, developed by Grunlan and colleagues, serves as a foundation for this dissertation.[11, 92, 109, 133] As pH of PEI is increased, its charge density decreases, causing the polymer to obtain a globular conformation leading to a thicker deposition of PEI (MMT pH was left unaltered at ~pH 9.7). The best oxygen barrier (corresponding with the thickest film) for 40 bilayers was found at pH 10 (0.34 $cm^3/(m^2 \cdot day \cdot atm)$ at 135 nm) OTR results as shown in Figure 13(a). In a later study, the concentration of MMT in solution was altered and it was found that transmission rate decreased as MMT concentration in suspension increased from 0.2% to 2%.[92] These 2% films showed the greatest performance with an OTR of 0.078 with only 20 bilayers, as shown in Figure 13(b). The films constructed with 2% MMT suspension, however, had slightly reduced transparency.

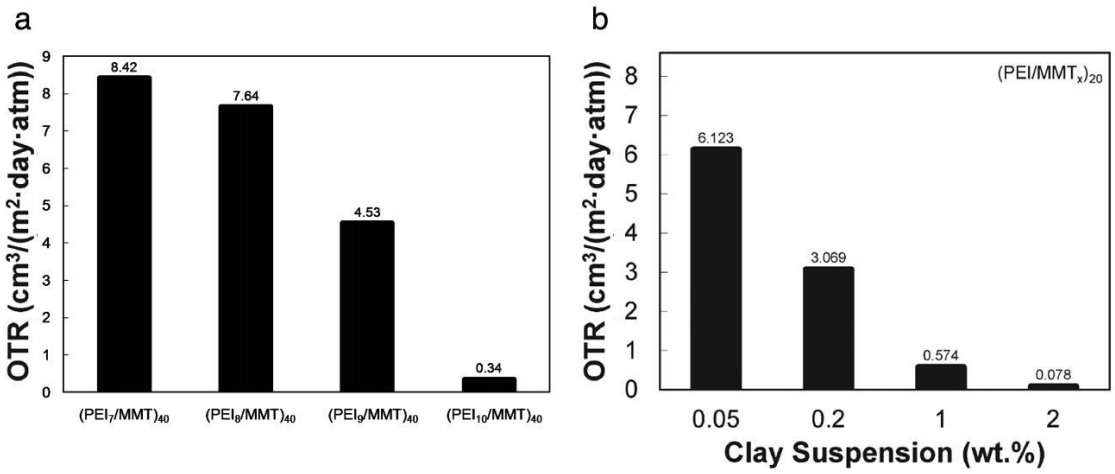

Figure 13. OTR results for (a) 40 BL of PEI_x/MMT_{10} with clay deposited from a 0.2 wt% suspension and (b) 20 BL PEI_{10}/MMT_{10} with various clay suspension loadings.[11, 92]

It was also discovered that a polymer-only system, PEI and poly(acrylic acid) [PAA], has significant gas barrier properties due to the high affinity of each polymer for the other creating a "scrambled salt" structure of the multilayer film.[15, 134] The T_g of this composite was well above the Wood and Fox estimates, suggesting very strong bonds between the polymers chains. In only 8 BL (451 nm thick) the film reached the undetectable level of commercial testing equipment, <0.005 $cm^3/(m^2 \cdot day \cdot atm)$. Various methods have been employed to reduce these films' sensitivity to moisture and even reduce out the transmission of water vapor, including crosslinking and using an alternative, less hydrophilic clay, vermiculite.[12, 15, 134-135] Carosio et. al. employed Nafion, a hydrophobic fluorinated polyanion, in conjunction with the PEI/MMT system to reduce the water vapor permeability of a poly(lactic acid) film by 75%.[136]

CHAPTER III

SHIFT-TIME ASSEMBLY: FAST FILM GROWTH AND HIGH GAS BARRIER BY ADJUSTING DEPOSITION TIME*

3.1 Introduction

Flexible gas barrier thin films are of particular interest for food packaging, pressurized systems, and flexible electronics encapsulation.[1-3] The metalized plastic film used for food packaging suffers from cracking and the inability to be microwaved, which could be solved by using LbL thin films. There are potential benefits of using light weight gas barrier films in various pressurized systems like sporting goods and aircraft. Flexible electronic displays require a good gas barrier to protect the underlying components from oxidative degradation. When considering implementation of layer-by-layer technology for these applications, the adage "time is money" holds true. In this case, it could be said that *processing time* is money. Layer-by-layer has traditionally been a slow process, with deposition times per layer ranging from 30 seconds to 25 min.[35, 40, 112-113, 115] Faster methods for deposition include spraying[115, 117, 137] and spin coating[119], but traditional immersion (or dipping) remains a viable option if shorter deposition times and fewer layers can be used. In an effort to reduce processing time, the "shift-time" method was

*Reprinted with permission from Hagen, D. A.; Foster, B.; Stevens, B.; Grunlan, J. C. Shift-Time Polyelectrolyte Multilayer Assembly: Fast Film Growth and High Gas Barrier with Fewer Layers by Adjusting Deposition Time. *ACS Macro Lett.* **2014**, 663-666.

developed to reduce the number of layers needed to achieve a desired property and reduce the exposure time for each layer. By reducing the processing time of initial layers, a sufficient film thickness to attain an undetectable oxygen barrier was constructed with fewer layers. This novel approach is illustrated in Figure 14.

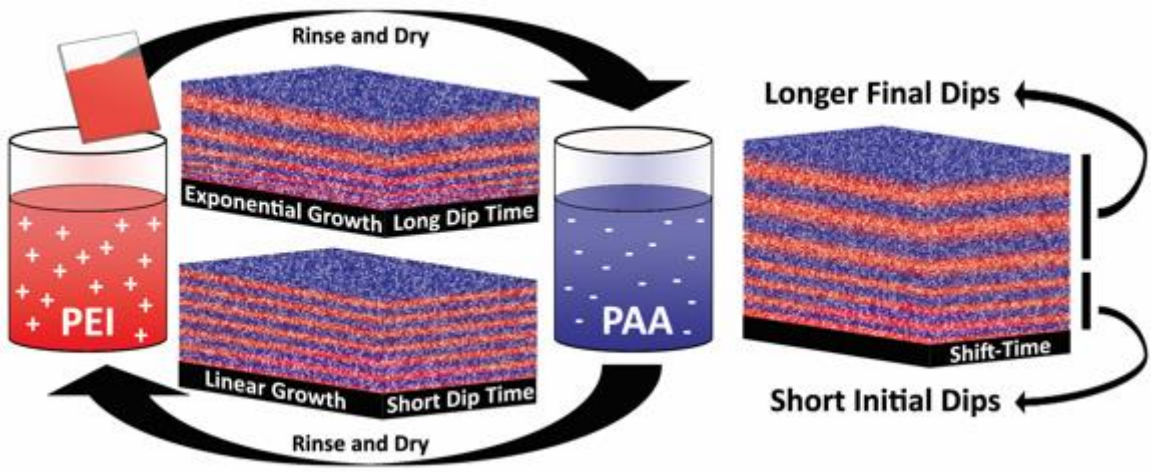

Figure 14. Schematic of the shift-time layer-by-layer dipping process used to achieve thicker films, with fewer layers, without altering the ingredients used.

3.2 Experimental

Poly(acrylic acid) (PAA) (M_w = 100,000 g/mol, ρ=1.20 g/cm^3), purchased from Sigma Aldrich (Milwaukee, WI), was used as a 0.2 wt% solution in DI water and adjusted to pH 4.0 using 1M NaOH. Branched polyethylenimine (PEI) (M_w = 25,000 g/mol, ρ=1.10 g/cm^3) was also purchased from Sigma-Aldrich and used as a 0.1 wt% DI water solution, adjusted to pH 10.0 using 1M HCl.

Poly(ethylene terephthalate) (PET) film, with a thickness of 179 μm (trade name ST505, produced by Dupont-Teijin), was purchased from Tekra (New Berlin, WI) and used as the substrate for oxygen transmission rate testing. This PET film has an OTR of approximately 9 $cm^3/(m^2 \cdot day \cdot atm)$ under dry conditions. Prior to deposition, PET substrates were rinsed with methanol and DI water, followed by treatment of each side of the substrate using a BD-20C Corona Treater (Electro-Technic Products, Inc., Chicago) to ensure an adequate negative surface charge. Polished silicon wafers were purchased from University Wafer (South Boston, MA) and were used as substrates for ellipsometry and profilometry. They were treated with piranha solution in a 3:1 mass ratio of 30% hydrogen peroxide to 99% sulfuric acid and stored in deionized (DI) water [*Caution! Piranha solution should be handled with extreme caution!*]. Silicon wafers were rinsed with acetone and DI water prior to deposition.

Each substrate was dipped into the cationic PEI solution for the designated dip time (i.e. one second or one minute). After this, and every subsequent dip, the substrate was pulled through a curtain of DI water at a speed of 25 mm/s to rinse off excess solution and then similarly dried with filtered air at a speed of 2.5 mm/s. The total time between each solution immersion was approximately 1 min. The substrate was then dipped into the anionic PAA solution for the same duration, which completed a single bilayer dipping cycle, as illustrated in Figure 14. For gradient deposition, 51 mm wafer sections were submerged into and immediately removed from solutions at a speed of 102 mm/min, so the resulting films were deposited with a linear gradient of dip times (0 to 1 min) along the wafer (Figure 15(b)). This method demonstrates the thickness trends, but actual

thickness values referenced in the text are taken from discrete wafers shown in Figure 15(a), which were constructed in the same manner as the films tested for OTR.

Thickness measurements were taken as a function of layers deposited using an α-SE spectroscopic ellipsometer (J.A. Woodlam Co, Inc., Lincoln, NE). For the gradient films, thickness was measured with a P-6 profilometer (KLA-Tencor, Milpitas, CA). Multiple scratches were made at each position so that height from the leveled substrate could be taken. All thickness values reported are an average of three measurements, and growth rates were calculated using linear regression. OTR testing was performed according to ASTM D-3985 specifications by MOCON (Minneapolis, MN) using an Oxtran 2/21 ML instrument at testing conditions of 23 °C and 0% RH.

3.3 Results and Discussion

The polyethylenimine (PEI)/poly(acrylic acid) (PAA) system has been shown to grow exponentially with one-minute dips when PEI is at pH 10 and PAA is at pH 4.[15] Each polymer is weakly charged at these pH levels, causing the polymer chains to assume a globular conformation due to minimal self-repulsion. For the deposition of PAA onto a PEI covered surface, the deposited PEI becomes highly charged in the pH 4 PAA solution, which requires more PAA to deposit to satisfy this charge. Likewise, the PAA surface also becomes highly charged in the alternate solution, causing more PEI to deposit. The complementary nature of these pH conditions allows for exponential growth. Eight PEI/PAA bilayers, deposited on a 175 μm PET substrate, is 651 nm thick and exhibits an undetectable oxygen transmission rate (OTR <0.005 $cm^3/(m^2 \cdot day)$), which is three orders of magnitude lower than uncoated PET.[15]

The influence of dip time on the growth of PEI/PAA assemblies was evaluated using a robotic system that dipped the entire substrate for the first n bilayers and then lessened the submersion depth incrementally for each successive bilayer.[138] This procedure created 6 mm stripes that allowed measurement of thickness as a function of bilayers deposited, as shown in Figure 15(a). The colors observed on the silicon wafers are the result of constructive interference of the light reflecting off the film surface and underlying silicon surface, where different colors indicate different thickness. In order to examine the influence of a continuous range of dip times (0-60 seconds), a deposition time gradient was generated along a single wafer by submerging and removing the entire wafer at a given speed, as shown in Figure 15(b). The thickness data from these wafers show that longer dip times create thicker films, which agrees with previous work where it was shown that the growth rate (i.e., thickness change per bilayer) is a result of the time-dependent polymer diffusion process.[35-36, 137] It should be noted that before these films reach a critical thickness, shorter dip times lead to thicker growth. These polymers deposit as coils, but as the films are held in solution some polymer chains are rejected from the surface. The remaining chains flatten onto the surface, obtaining a more thermodynamically stable conformation with more of the charged groups paired with surface charges.[139] As layers are deposited, diffusion into the film allows for much thicker deposition, but the relaxation phenomenon causes the longer dip times to have a very slow initial growth period. For exponentially growing LbL films, the growth rate increases as bilayers are deposited due to the additional amount of underlying film into which the polymer can diffuse. When the film no longer becomes saturated at a given deposition

time, the growth transitions from exponential to linear. The final linear growth rate is diffusion limited, with longer depositions providing larger growth rates.[35] For the films deposited in shorter intervals, there is almost no transition, and the final linear growth is obtained after only 3 bilayers. These films have the highest growth rate for the first few bilayers due to a limited time for chain relaxation, leaving a thick tightly-coiled layer. Although they reach this final linear growth regime with the fewest number of BL, the shorter dip time films have the smallest final growth rate due to limited diffusion of polymer into the underlying film.

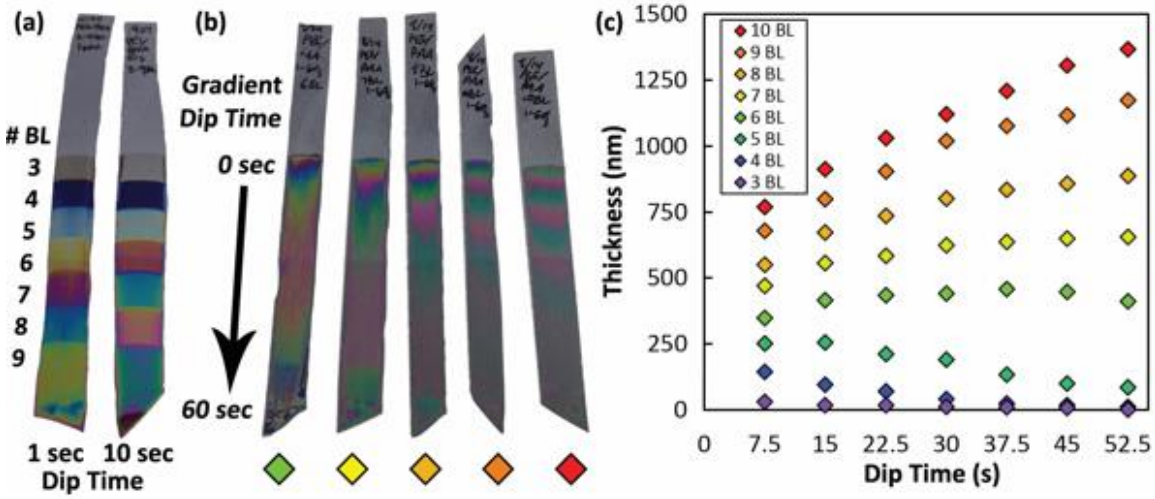

Figure 15. Images of PEI/PAA thin film assemblies on silicon wafers with (a) different dip times for each wafer and stripes of different bilayers and (b) wafers of different numbers of bilayers with a gradient of dip time. (c) Profilometer thickness of gradient wafers at different numbers of bilayers. Colored diamonds in (b) correspond to the same colors in (c). This thickness data was acquired with profilometry.

The shift-time method takes advantage of the high initial growth rate of the short deposition time and the high linear growth of the longer deposition time by initiating the film growth with a short dip time and then transitioning to a longer dip time. One-second and one-minute exposures are used because these correspond to the extrema of the trends observed within this time domain. The first four bilayers were deposited with one-second dips to quickly build enough material to support the full diffusion of one-minute dips. Figure 16 shows that the growth rate of the shift-time film (260 nm/BL), during one-minute dips, nearly matches that of the film that was constructed entirely with one-minute dips (280 nm/BL), but shift-time achieved a similar thickness with two fewer bilayers, 650 nm at 8 BL and 552 nm at 6 BL, respectively. Furthermore, the total deposition time for 8 bilayers with one-minute dips is 16 minutes, while a 6 BL shift-time assembly, having comparable thickness, reduced deposition time to approximately 4 minutes.

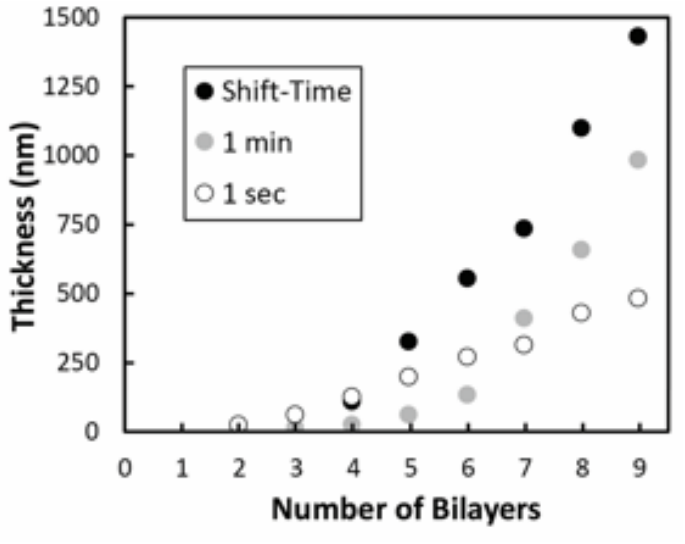

Figure 16. Thickness as a function of PEI/PAA bilayers deposited with one-minute, one-second, and shift-time depositions, where the first 4 BL of the shift-time film are one second and the succeeding layers are one minute. This thickness data was acquired with ellipsometry.

Figure 17 shows oxygen transmission rate as a function of bilayers deposited. The films deposited with one-second dips show an order of magnitude improvement over the bare PET substrate at four bilayers, while the films produced with one-minute deposition showed relatively little improvement due to the thin growth through five bilayers. The shift-time film shows a significant improvement in barrier performance from the 4th to the 5th bilayer, which is its first one-minute deposition BL. Only shift-time assemblies achieve the undetectable OTR limit of 0.005 $cm^3/(m^2 \cdot day)$ at 6 BL, which is more than 3 orders of magnitude lower than over the 179 μm PET substrate. This 552 nm thick film exhibits the greatest oxygen barrier reported in the literature for an LbL film comprised of 12 (or fewer) total layers (i.e., 6 BL). In many cases, the OTR achieved with five bilayers (0.016

$cm^3/(m^2 \cdot day)$) would be enough for many packaging applications and could be deposited roll-to-roll with a flexographic or multilayer slot printer.[140]

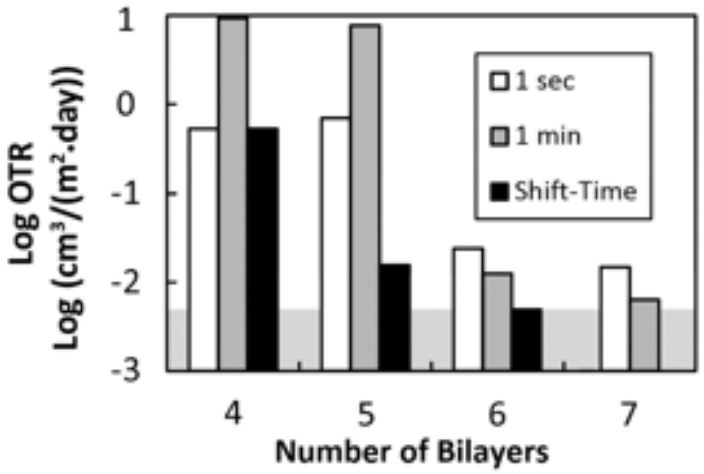

Figure 17. Oxygen transmission rate as a function of PEI/PAA bilayers deposited with one-minute, one-second, and shift-time dips, where the first 4 BL of the shift-time film are one second and the succeeding layers are one minute. The shaded background represents the undetectable range of OTR testing equipment (<0.005 $cm^3/(m^2 \cdot day)$).

3.4 Conclusions

The shift-time method presented here is a novel way of taking advantage of the various methods in which polyelectrolytes are deposited in an exponentially growing system. By understanding the initial adsorption and relaxation driving forces in the initial layers and the effect of diffusion of a polymer into a film after substantial material is deposited, the 6 BL shift time-film was able to perform as well as the normal 8 BL film, while reducing the deposition time by 73%. These results, in addition to the myriad of useful properties that can be obtained with LbL thin films, should aid in the adoption of layer-by-layer into commercial processes.

CHAPTER IV

SIMILARLY CHARGED MULTILAYERS*

4.1 Introduction

The LbL process has been used to create very good barriers using bilayer (BL) and quadlayer (QL) systems that utilize impermeable nanoplatelets (e.g., clay and graphene oxide), each approximately 1 nm thick with aspect ratios up to several thousand, to create an extremely tortuous pathway for diffusion of gas molecules.[11-16] The water based nature of the layer-by-layer process allows for partially exfoliated and oriented clay platelets to be deposited every cycle, generating a nanobrick wall structure. This structure provides superior properties over bulk composites where aggregation and random orientation lead to increased opacity and greater gas permeability.[13] The traditional method of constructing LbL thin films involves alternately depositing layers from oppositely charged solutions.[10] One disadvantage of this approach is the incomplete coverage of a surface due to the rigidity of clay platelets. In the present study, we show that succeeding the anionic clay layer with a similarly charged polymer layer significantly improves the gas barrier by filling in the gaps between clay platelets of the same layer. A trilayer (TL) system consisting of the cationic polyethylenimine (PEI), anionic montmorillonite clay (MMT), and anionic poly(acrylic acid) (PAA) is used to create super gas barrier nanobrick walls. A trilayer system, similar to that examined here has recently been studied to

---

combine the exponential growth of all polymer systems with the flame retardant behavior of montmorillonite clay.[142] Our focus here, however, is on gas barrier properties. At comparable thickness to PEI/MMT bilayers, these PEI/MMT/PAA trilayers achieve an oxygen transmission rate that is more than an order of magnitude lower.

4.2 Experimental

4.2.1 Materials

Natural sodium montmorillonite clay (MMT, trade name Cloisite NA+) provided by Southern Clay Products, Inc. (Gonzales, TX), was dispersed as a 1 wt% suspension in deionized (DI) water by rolling solutions in bottles overnight. MMT platelets have a reported density of 2.86 g/cm^3, diameter ranging from 10-1000 nm, and thickness of 1 nm.[143] Poly(acrylic acid) (PAA) (Mw = 100,000 g/mol, ρ=1.20 g/cm^3), purchased from Sigma Aldrich (Milwaukee, WI), was used as a 0.2 wt% solution in DI water. Branched polyethylenimine (PEI) (M_w = 25,000 g/mol, ρ=1.10 g/cm^3) was also purchased from Sigma-Aldrich and used as a 0.1 wt% DI water solution.

4.2.2 Substrates

Poly(ethylene terephthalate) (PET) film, with a thickness of 179 μm (trade name ST505, produced by Dupont-Teijin), was purchased from Tekra (New Berlin, WI) and used as the substrate for oxygen transmission rate (OTR) testing and transmission electron microscopy (TEM). This PET film has an OTR of approximately 8.6 cm^3/(m^2·day·atm) under dry conditions. Polished silicon wafers were purchased from University Wafer (South Boston, MA) and were used as substrates for ellipsometry and atomic force microscopy. They were treated with piranha solution in a 3:1 mass ratio of 30% hydrogen

peroxide to 99% sulfuric acid and stored in deionized (DI) water [Caution! Piranha solution should be handled with extreme caution!]. Silicon wafers were rinsed with DI water, acetone, and then DI water immediately before use. Prior to deposition, PET substrates were rinsed with DI water, methanol, and then DI water, followed by treatment of each side of the substrate using a BD-20C Corona Treater (Electro-Technic Products, Inc., Chicago) to ensure an adequate negative surface charge before coating.

4.2.3 Layer-by-Layer Assembly

Each substrate was dipped into the cationic 0.1 wt% PEI solution (adjusted to pH 10.0 using 1 M HCl) for 5 minutes. After this, and every subsequent dip, the substrate was rinsed with DI water and dried with filtered air. The substrate was then dipped into the anionic MMT suspension (unaltered pH of ~9.7) for five minutes, which completed a single bilayer (BL) dipping cycle, as illustrated in Figure 18. When depositing trilayer films, the substrate was dipped into the anionic PAA solution (adjusted to pH 4.0 using 1M NaOH) for 1 minute to complete a TL cycle. All subsequent dips were 1 minute, following the sequence described above. After the final rinsing and air drying, the films deposited on PET were dried in an oven at 70°C for 15 min.

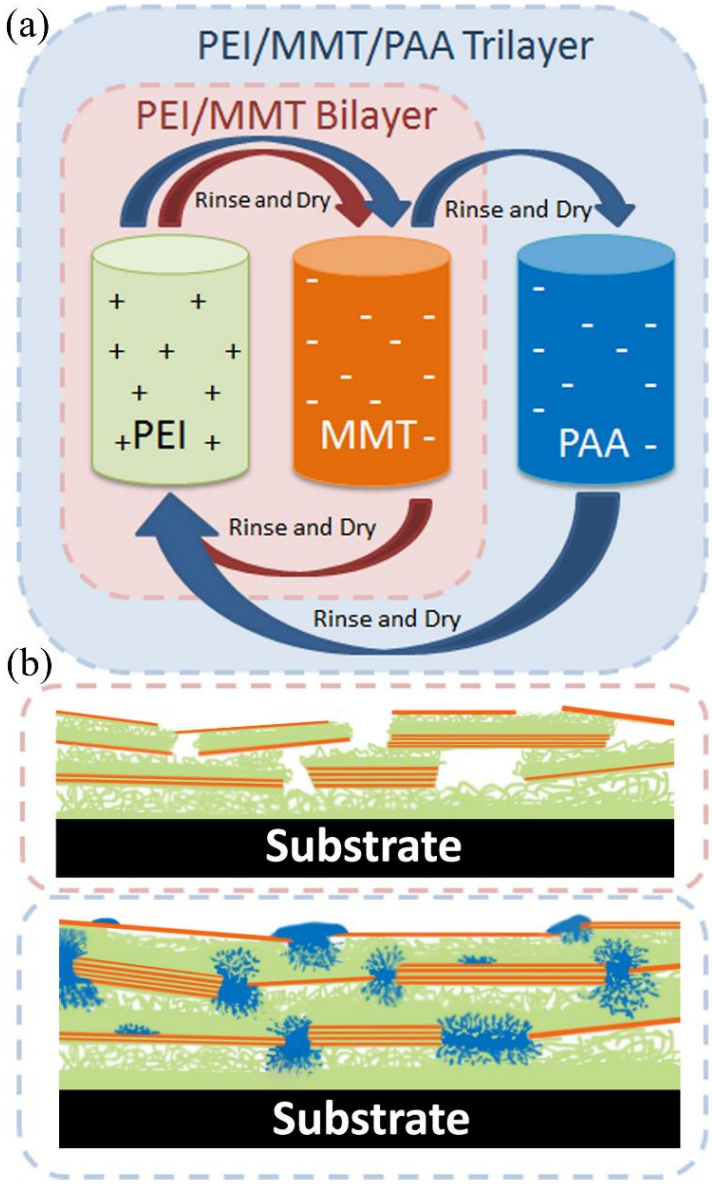

Figure 18. Illustrations of (a) the LbL dipping process and (b) nanobrick wall structures built from alternate adsorption of PEI (green) and MMT (orange) for the BL system (top) and PEI, MMT, and PAA (blue) for the TL system (bottom).

4.2.4 Characterization

Thickness measurements were taken as a function of layers deposited using an α-SE spectroscopic ellipsometer (J.A. Woodlam Co, Inc., Lincoln, NE). Mass deposition onto Ti/Au plated quartz crystals was measured using a Research Quartz Crystal Microbalance (QCM) (Maxtek Inc., Cypress, CA). Density was calculated by dividing the mass/area obtained with QCM by the film thickness. Data for clay mass deposition were taken between 10 and 20 cycles to avoid substrate effects. Visible light was measured using a USB2000-UV−Vis Spectrometer (Ocean Optics, Dunedin, FL). Atomic force microscopy data (AFM) was acquired using a Dimension Icon AFM (Bruker, Billerica, MA) in tapping mode with an HQ:NSC35/Al BS probe (Mikromasch, Lady's Island, SC). Root mean square roughness (rms) measurements were taken from a 20μm x 20μm area. OTR testing was performed according to ASTM D-3985 specifications by MOCON (Minneapolis, MN) using an Oxtran 2/21 ML instrument at testing conditions of 23 °C and 0% RH. Samples for TEM were prepared by embedding the film in Epofix (EMS, Hatfield, PA) resin overnight and cutting sections, using an Ultra 45° diamond knife (Diatome, Hatfield, PA), onto 300 mesh copper grids. TEM micrographs of the thin film cross sections (~90 nm thick) were imaged using a Tecnai G2 F20 (FEI, Hillsboro, OR) at an accelerating voltage of 200kV.

4.3 Results and Discussion

4.3.1 Film Growth

Figure 19 compares the thickness of PEI/MMT bilayers and PEI/MMT/PAA trilayers. The polymer/clay bilayers increase in thickness linearly at 4.0 nm/BL (Figure

19(a)). When PAA is employed as a third layer in each deposition cycle, the growth rate increases slightly to 5.2 nm/TL for two reasons. PAA deposits onto the exposed areas of PEI between MMT platelets via electrostatic attraction. Any exposed PEI is at a more highly charged state in the PAA solution (pH 4) than it was in the MMT solution (pH 9.7), aiding in the attraction of PAA. Secondly, PAA carbonyls can hydrogen bond with MMT hydroxyl groups at low pH due to the minimal electrostatic repulsion between weakly-charged PAA chains and MMT platelets.[142, 144-145] PAA fills in the gaps of the MMT layer which provides a more uniform, negatively charged surface on which the following layer of PEI can deposit, which contributes to the increased thickness of the trilayer system.

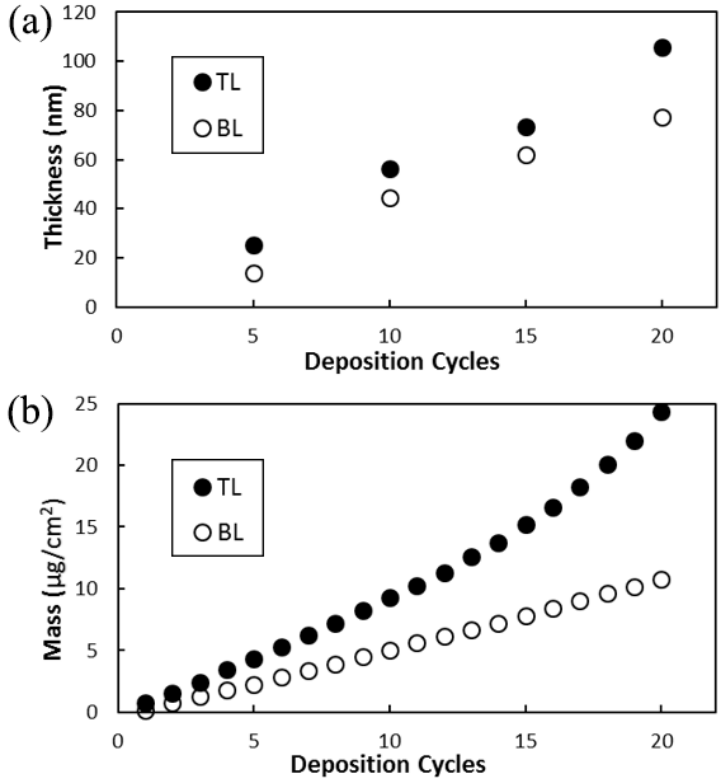

Figure 19. (a) Thickness and (b) mass of PEI/MMT bilayer and PEI/MMT/PAA trilayer systems as a function of deposition cycles.

The mass of the trilayer film per cycle is significantly greater than that of the bilayer film (Figure 18(b)) due to PAA occupying free volume that cannot be filled by the relatively large, rigid clay platelets. This higher packing efficiency for the trilayer system is verified by examining the density of both thin films. After 20 cycles the bilayer system has a density of 1.39 g/cm^3, compared to a density of 2.30 g/cm^3 for the trilayer system. In addition to filling in voids between MMT platelets, PAA can diffuse into underlying PEI layers via an in and out diffusion mechanism that is commonly observed in exponentially growing thin films.[33, 146-147] A previous study showed that a 10 BL film of

PEI/PAA has a thickness greater than 1 μm and a mass of approximately 140 μg/cm^2 due to the large amount of diffusion of each of the polymers into the film.[15] The thickness and mass of this all-polymer system are more than an order magnitude greater than that of the clay filled TL system. This is because PAA cannot diffuse directly through the MMT platelets, which inhibit the exponential growth observed in the all polymer system.[12] However, the exposed areas of PEI between clay platelets allow some diffusion of PAA into the film which could increase the mass of the system. The subsequent layer of PEI not only has a smooth anionic surface of MMT and PAA on which to deposit, but also has soft areas of PAA into which it can diffuse, whereas in the PEI/MMT bilayer, it is only attracted to the MMT covered surface. In the previous study of this trilayer system (for flame retardant properties), in which a 0.2 wt % solution of clay was used, the mass of 10 TL was approximately five times the mass of the 10 TL system measured here. This is presumably due to a lower number of clay platelets being deposited and increased diffusion of PAA into the underlying PEI. In the present study, there is an average of 65% more clay deposited in the TL system per cycle than in the BL system (0.84 μg/cm^2 and 0.51 μg/cm^2 respectively, Figure 20) which means there is better lateral packing of clay platelets and/or more platelets (or stacks) deposited on top of each other every layer. This is most likely a result of a more uniform PEI layer that deposits onto the MMT/PAA surface, where the bilayer system may have gaps in the coverage resulting in a lower net attraction of MMT platelets (illustrated schematically in Figure 18(b)).

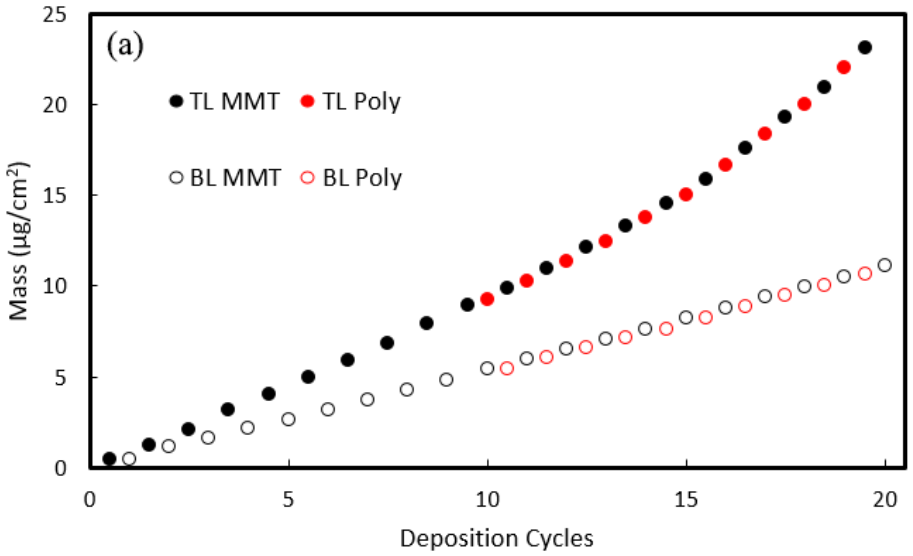

Figure 20. (a) Thin film mass after polymer and MMT depositions for the bilayer (PEI/MMT) and trilayer (PEI/MMT/PAA) systems and (b) the same systems using high molecular weight PEI.

Interestingly, if the order of MMT and PAA is switched (e.g. PEI/PAA/MMT) the film's morphology changes completely. The thickness of this reversed trilayer system is the same as that of PEI/PAA, and no additional mass is detected during the MMT deposition. Therefore, we conclude that MMT does not deposit onto a PAA covered surface at the given pH conditions. At the supramolecular level, the PAA-MMT attraction could stem from either electrostatic interaction or hydrogen bonding; given that they are both negatively charged, the electrostatic force is repulsive. PAA, unlike the relatively large MMT platelets, completely covers and uniformly reverses the charge of the PEI covered surface, leaving no exposed PEI to attract MMT.[15] Furthermore, hydrogen bonding between PAA and MMT does not occur at the high pH condition (9.7) of the

MMT solution due to PAA becoming highly charged.[142, 144-145] Therefore, MMT platelets are repelled from the surface in the PEI/PAA/MMT coating sequence.

4.3.2 Film Morphology

TEM images of a microtomed 20 TL film (Figure 21 (a-c)) highlight the high level of ordering of these nanobrick walls. Montmorillonite clay platelets, about 1 nm thick and 100 nm in diameter,[143] possess high electron density due to the aluminum, magnesium and silicon atoms that cause them to appear as dark lines in these images. The polymers present (PEI, PAA, supporting PET film, and epoxy support) have much lower electron density and therefore appear brighter in the micrographs. There are many more clay platelets seen (~45-Figure 21(a)) through the thickness of the film than there were deposition cycles (20), which demonstrates that each deposition cycle does not deposit only one discrete layer of clay platelets along the surface. It is likely that doublet and triplet stacks of clay platelets are deposited every cycle, due to only partial exfoliation in solution, and the mobility of the successive polymer is high enough to intercalate these stacks on the surface. A stack of 5 MMT platelets is shown (Figure 21(c), bottom, dashed). The stack is deposited at the bottom of the film with no platelets directly to its left. A second stack of three platelets appears higher in the image and does not align with the surrounding platelets. The average thickness of the 20 TL film as measured from TEM images (94 ± 13 nm (n=50)) is in good agreement with ellipsometry measurements (Figure 19(a)). The clay platelet spacing within the film is rather uniform, as demonstrated by the Fourier Transform analysis taken from the entire thickness of the image (Figure 21(a) inset). The TEM images of the bilayer film reveals highly aligned platelets, but also lighter

areas between some of the clay platelets indicating gaps in the nanobrick wall structure (Figure 21(d)).

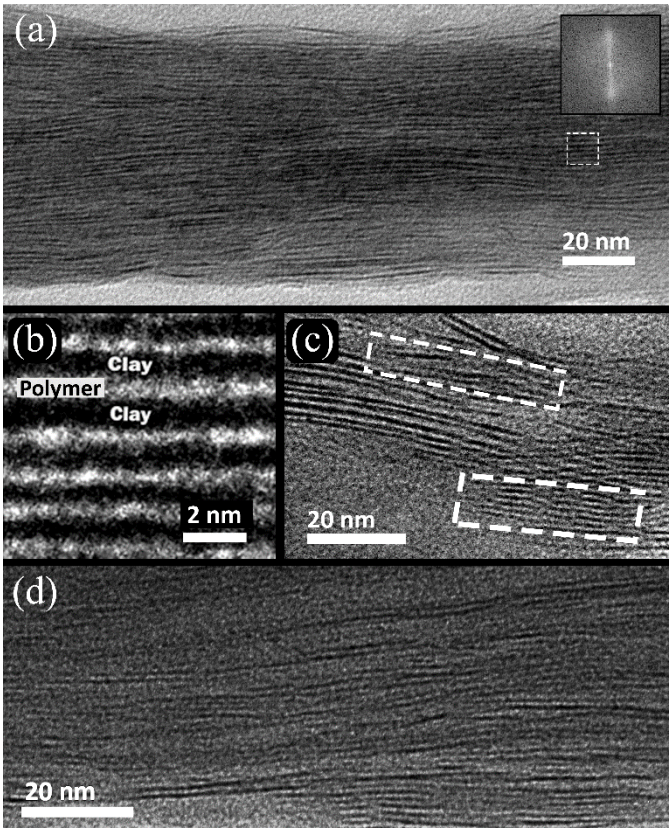

Figure 21. (a) TEM cross section of a 20 PEI/MMT/PAA trilayer film prepared using a microtome and Fourier Transform inset. The white rectangle in (a) is shown at higher magnification in (b), and stacks of MMT platelets within the film are shown in (c). (d) Cross section of part of a 20 BL film.

The bilayer film surface is rougher than the trilayer surface (rms roughness values of 19.5 nm and 15.7 nm, respectively) due to PAA filling in the gaps between MMT platelets, as illustrated in Figure 18(b). The surface of a 10 trilayer film was imaged before

and after the final PAA depostion to demonstrate the partial deposition of PAA onto a the MMT surface. AFM phase images represent the phase shift (delay) of the cantelever compared to its free oscillation. This delay can be caused by soft or viscoelestic materials,[148] such as PAA, that appears as lighter areas in Figure 22. There is a stark contrast between the phase images between the MMT covered surface and the MMT/PAA covered surface (Figure 22), which should not be confused with topogrophy (the surface is in fact slightly rougher before the PAA deposition). There are regions where the PAA deposition is less concentrated, which could be areas of greater clay platelet coverage and PAA is only attracted to the surface via hydrogen bonding.

It should be noted that a 20 TL film, with a thickness of 106 nm, has an average light transmission of 95% across the visible light spectrum (390-750 nm). This high level of transparency is a key requirement for electronic display encapsulation and is desirable for many food packaging applications.[3] It is the high level of orientation of the clay within the composite film that makes this exceptional transparency possible.

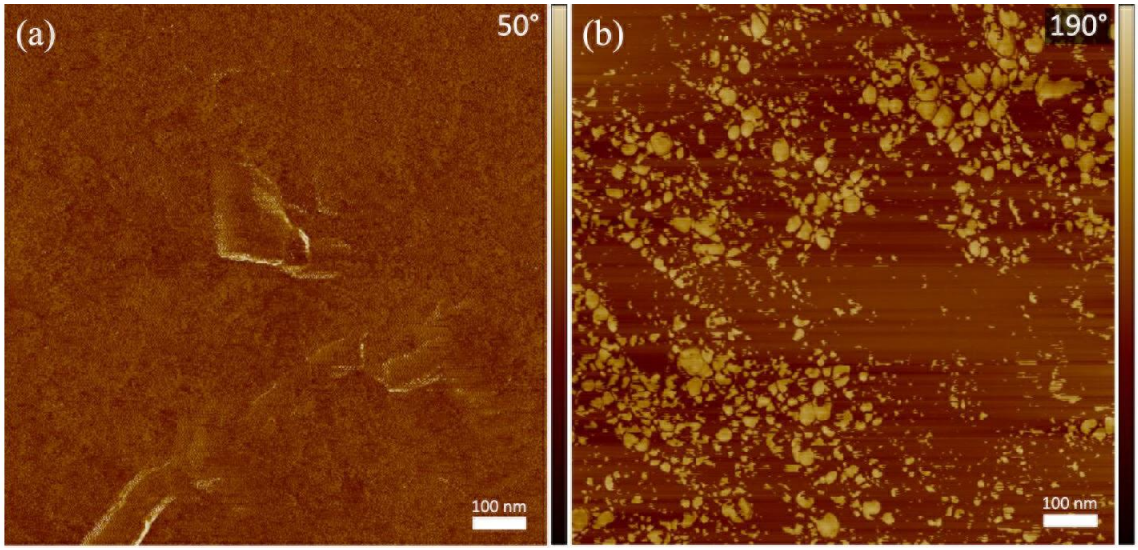

Figure 22. AFM phase images of 10 TL of PEI/MMT/PAA (a) before the final layer of PAA is deposited and (b) with the final layer of PAA deposited.

4.3.3 Gas Barrier Properties

The difference in gas barrier properties between the bilayer and trilayer nanobrick walls is more pronounced than the differences in thickness and mass (Figure 19). Oxygen transmission rates for both systems are summarized in Figure 23. While 5 BL shows only a small reduction in oxygen transmission rate over the bare PET support (OTR is 7.3 and 8.5 $cm^3/m^2 \cdot day$, respectively), the 5 TL thin film shows nearly a factor of three improvement. Furthermore, a 10 TL film has lower OTR than 20 BL despite having half as many clay depositions. 20 TL is at the detection limit of commercial equipment (0.005 $cm^3/m^2 \cdot day$), a 1600× improvement over 179 μm PET (8.6 $cm^3/(m^2 \cdot day \cdot atm)$). The OTR of 20 TL is nearly one order of magnitude lower than that of 20 BL.

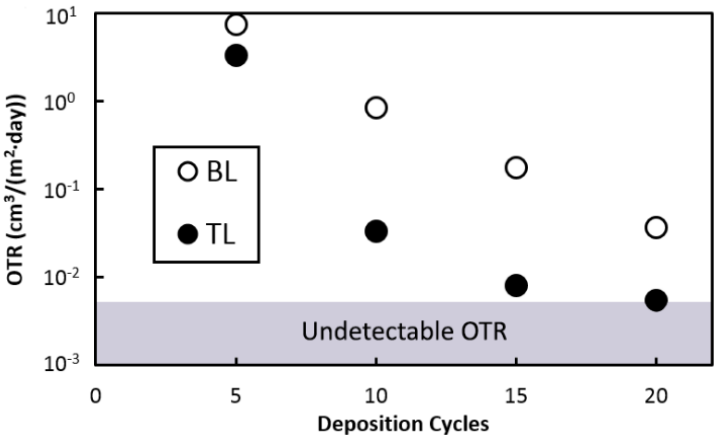

Figure 23. Oxygen transmission rates for PEI/MMT bilayers and PEI/MMT/PAA trilayers as a function of bilayer or trilayer sequences deposited.

This improvement comes from the inclusion of more clay platelets per deposition cycle and also from the free volume reduction discussed previously, which slows the diffusion of oxygen molecules through the film. Having more platelets deposited every cycle provides smaller gaps between platelets on the same plane and/or more platelets to diffuse around vertically. Both of these scenarios create a more tortuous path for oxygen molecules, leading to better barrier performance. The permeability of the 20 TL film is extremely low (1.21×10^{-21} ($cm^3 \cdot cm/cm^2 \cdot s \cdot Pa$) in Table 2) at a thickness of only 105.8 nm. Thin film permeability is decoupled from the substrate permeability using a previously described method.[89]

Table 2. Thickness, oxygen transmission rate, and film permeability for PEI/MMT BL and PEI/MMT/PAA TL systems.

	Film Thickness (nm)		OTR ($cm^3/m^2 \cdot day$)		Film Permeability ($cm^3 \cdot cm/cm^2 \cdot s \cdot Pa$)	
Cycles	TL	BL	TL	BL	TL	BL
5	25.3	13.8	3.271	7.316	3.08×10^{-19}	1.68×10^{-18}
10	56.3	44.5	0.034	0.843	4.39×10^{-21}	9.52×10^{-20}
15	73.2	61.9	0.008	0.175	1.34×10^{-21}	2.53×10^{-20}
20	105.8	77.4	0.005	0.037	1.21×10^{-21}	6.57×10^{-21}

4.4 Conclusions

Here it was shown that that the addition of a polymer layer with similar charge as clay fills uncovered spaces in the nanobrick wall and dramatically increases oxygen barrier properties by reducing the free volume. The exceptionally high oxygen barrier exhibited, coupled with high transparency, ease of fabrication, and mechanical flexibility, makes these films well suited for pressurized systems, food packaging, and flexible electronics.

CHAPTER V

CONTROLLING PACKING OF CLAY BY ALTERING PH*

5.1 Introduction

There are many parameters that can be altered during deposition of layer-by-layer thin films to further tailor the final thin film morphology (concentration, pH, solution temperature, ionic strength, charge density, molecular weight, and polymer chain architecture).[10, 101] In the LbL literature, many studies have examined the influence of polyelectrolyte solution pH on the resultant thin film growth rate and morphology.[11, 36, 149-150] In addition to changing the charge density and resultant configuration of the polymer in an aqueous solution, altering one solution pH will also affect the charge density of the exposed polymer chains of the previously deposited layer.[15, 151-152]

The present study shows that altering pH of the aqueous clay suspension changes the amount of clay deposited in the nanobrick wall structure (i.e., clay nanoplatelet bricks and polymer mortar). In the case of montmorillonite (MMT) clay platelets, charge density does not dramatically change with regard to suspension pH, but altering the pH of the clay alters the previously deposited polyethylenimine (PEI) layer. PEI is very highly charged at low pH and has only a low charge density at high pH.[153] Thicker polymer layers are deposited at pH 10 because PEI assumes a coiled conformation due to minimal self-

---

*Reprinted with permission from Hagen, D. A.; Saucier, L.; Grunlan, J. C. Controlling Effective Aspect Ratio and Packing of Clay with pH for Improved Gas Barrier in Nanobrick Wall Thin Films. *ACS Appl. Mater. Interfaces* **2014,** *6* (24), 22914-22919. Copyright 2014 American Chemical Society.

repulsion in its low charge state.[11] MMT generates a basic pH (~10) in water, but adjusting it to a lower pH causes the previously deposited PEI to become highly charged, driving more clay to be deposited. An increase in the thickness of PEI/MMT bilayers (BL), as the MMT suspension pH is reduced, is shown schematically in Figure 24(a). More clay in each deposited layer leads to exceptional oxygen barrier, and these nanobrick wall structures (MMT bricks with PEI mortar) also exhibit flexibility and high transparency that are desirable in barrier applications for food packaging, flexible electronics, and pressurized bladders.[1-3] Traditional barrier layers, such as metallized plastic or inorganic oxides (e.g., SiO_x), require complex processing and are prone to cracking and pinholes.[5-6] The polymer-clay nanocomposite thin films explored here are capable of reducing the amount of material used, while providing a more aesthetic (transparent) film, using a lower energy and environmentally-friendly process.

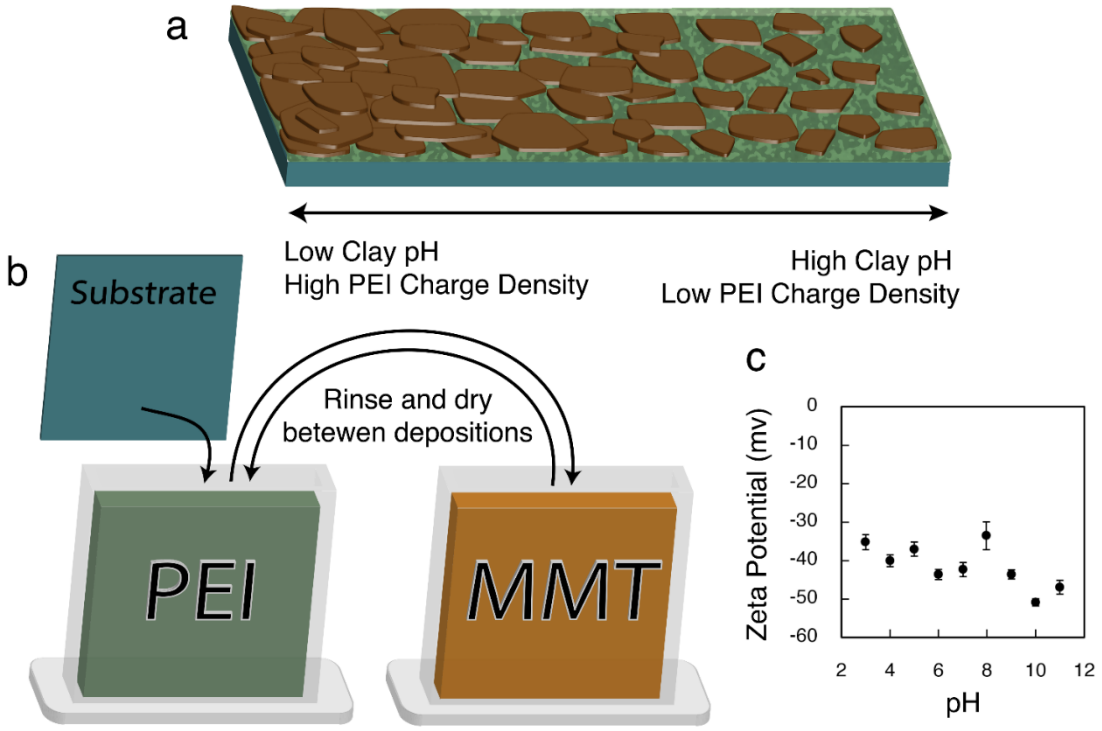

Figure 24. (a) Illustration of clay deposition onto PEI surface as a function of clay suspension pH, (b) schematic of layer-by-layer deposition process, and (c) zeta potential of MMT clay as a function of pH.

5.2 Experimental

5.2.1 Materials

Branched polyethylenimine (M_w = 25,000 g/mol, ρ=1.10 g/cm^3) was purchased from Sigma-Aldrich (St. Louis, MO) and used as a 0.1 wt% DI water solution. Natural sodium montmorillonite clay (trade name Cloisite NA+), provided by Southern Clay Products, Inc. (Gonzales, TX), was dispersed as a 1 wt% suspension in deionized (DI) water by rolling in bottles overnight. MMT platelets have a reported density of 2.86 g/cm^3, diameter ranging from 10-1000 nm, and thickness of 1 nm.[143] Zeta potential of MMT

suspensions was measured with a Zeta Phase Angle Light Scattering (ZETA PALS) instrument (Brookhaven Instruments Corporation, Holtsville, NY).

5.2.2 Substrates

Poly(ethylene terephthalate) (PET) film, with a thickness of 179 μm (trade name ST505, produced by Dupont-Teijin), was purchased from Tekra (New Berlin, WI) and used as the substrate for oxygen transmission rate (OTR) testing and transmission electron microscopy (TEM). This PET film has an OTR of approximately 8.6 $cm^3/(m^2 \cdot day \cdot atm)$ under dry conditions.[11] Prior to deposition, PET substrates were rinsed with methanol and DI water, followed by treatment of each side of the substrate using a BD-20C Corona Treater (Electro-Technic Products, Inc., Chicago, IL) to ensure an adequate negative surface charge before coating. Polished silicon wafers, purchased from University Wafer (South Boston, MA), were used as substrates for profilometry and atomic force microscopy (AFM). Silicon wafers were rinsed with acetone and DI water and then plasma treated for five minutes immediately before use. Thin films to be used for thermogravimetric analysis (TGA) were deposited onto polytetrafluoroethylene (PTFE) sheets purchased from McMaster-Carr (Elmhurst, IL). The PTFE sheets were rinsed with ethanol and water, but corona treatment was omitted to cause weaker adhesion and ultimately produce freestanding films.

5.2.3 Layer-by-Layer Assembly Procedure

All deposition was carried out at room temperature by an automated dipping system.[138] Each substrate was dipped into the cationic 0.1 wt% PEI solution (adjusted to pH 10.0 using 1 M HCl) for one minute. After this, and every subsequent dip, the substrate

was rinsed with DI water and dried with filtered air. The substrate was then dipped into a 1 wt% anionic MMT clay suspension for one minute (adjusted using 1M HCl), which completed a single bilayer (BL) dipping cycle, as illustrated in Figure 24(b). This process was repeated until *x* bilayers were obtained, denoted as $[PEI_{10}/MMT_y]_x$, where *y* is the MMT suspension pH. After the final rinsing and air drying, the films deposited onto PET were dried in an oven at 70°C for 15 min.

5.2.4 Thin Film Characterization

Film thickness was measured as a function of bilayers deposited with a P6 profilometer (KLA-Tencor, Milpitas, CA). Multiple scratches were made through each film so that height from the leveled substrate could be measured, and each data point reported is an average of values from three wafers. Mass deposition onto Ti/Au plated quartz crystals was measured using a Research Quartz Crystal Microbalance (QCM) (Maxtek Inc., Cypress, CA) by measuring the resonant frequency value of the crystal after every drying step. Atomic force microscopy (AFM) was performed with a Dimension Icon AFM (Bruker, Billerica, MA) in tapping mode with an HQ:NSC35/Al BS probe (Mikromasch, Lady's Island, SC). Root mean square roughness (R_q) measurements were taken from a 20µm x 20µm area. TGA was performed with a Q50 Thermogravimetric Analyzer (TA Instruments, New Castle, DE). 200 BL films on PTFE substrates were soaked in DI water overnight and scraped off using a razor blade in a sweeping motion to ensure the substrate was not scraped off with the film. The film was heated at 10°C/min to 120°C and held for an hour to remove all excess moisture. The film was then heated at the same rate to 650°C and held for an hour. Clay concentration was calculated as the mass

remaining at the end of the test divided by the mass at the end of the 120°C holding period. OTR testing was performed according to ASTM D-3985 specifications by MOCON (Minneapolis, MN) using an Oxtran 2/21 ML instrument at 23 °C and 0% RH. Samples for TEM were prepared by embedding the film in Epofix resin (EMS, Hatfield, PA) overnight and cutting sections, using an Ultra 45° diamond knife (Diatome, Hatfield, PA) at a 6° angle, onto 300 mesh copper grids. TEM micrographs of the thin film cross sections (~90 nm thick) were imaged using a Tecnai G2 F20 (FEI, Hillsboro, OR) at an accelerating voltage of 200kV.

5.3 Results and Discussion

5.3.1 Influence of pH on Film Growth

Using two polymers that have inherently low charge densities in their own solution, but become highly charged when exposed to the pH condition of the other solution, allows for very thick multilayer growth.[15] The high surface charge of the previously deposited polymer layer causes a thick deposition of the following layer in order to satisfy this imparted charge. This technique has primarily been used for weak polyelectrolytes,[101] but the same concept can be used to increase the growth rate of a polymer/nanoparticle system.[151] In the present study, PEI at pH 10 is combined with MMT at varying pH. Figure 24(c) shows that the zeta potential of MMT platelets in aqueous suspension is not highly dependent upon pH, fluctuating between -30 and -50 mV in the pH range of 3-11, which is due to the dominating permanent negative charge of the MMT platelet basal planes (as a result of isomorphic substitutions).[154] The amphoteric edge sites are positively charged below and negatively charged above pH 6.5, but have

only a small influence on zeta potential.[154] In contrast, polyethylenimine charge density is highly dependent upon pH.[153] At pH 10 there is less than 5% protonation, but many of the amine groups become protonated as the pH decreases (approximately 60% protonation at pH 4).[153]

In an effort to deposit more MMT platelets in a given deposition cycle, the pH of the clay suspension was reduced, which dramatically increased the charge density of the previously deposited PEI layer. This increase in charge density attracts more clay platelets to the surface, creating a thicker, more densely-packed layer, shown schematically in Figure 24(a). The $PEI_x/MMT_{9.7}$ (the unaltered MMT suspension is pH 9.7) system was previously studied to examine the influence of PEI pH on film growth.[11] The thickest growth was achieved at pH 10, with a linear growth rate of approximately 3 nm/BL through 20 BL. The growth of PEI_{10}/MMT_x is shown in Figure 25(a) to be significantly greater as the pH of the MMT suspension decreases, due to an increased amount of MMT deposited.

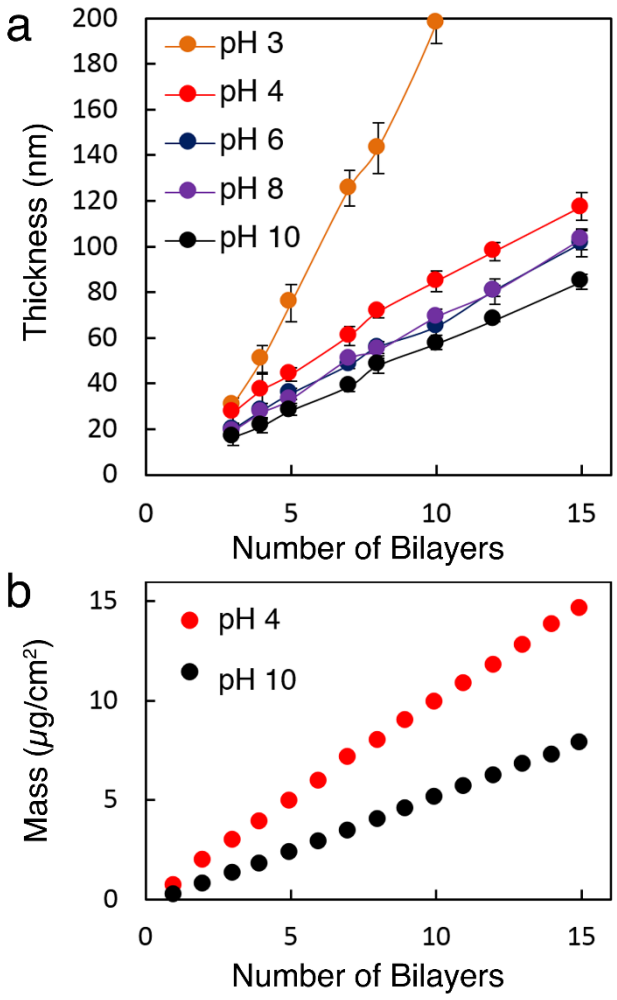

Figure 25. (a) Thickness of pH 10 PEI deposited with MMT of varying pH. The lines shown are simply a guide for the eye. (b) Mass deposition of PEI_{10}/MMT_x at clay pH of 4 and 10.

QCM reveals a significant increase in mass deposited for the lower pH clay system, shown in Figure 25(b). Clay concentration of the film could not be calculated using QCM due to instances where the total mass was reduced after the PEI deposition, from desorption of some of the outermost clay platelets (and replacement by PEI of less mass).

Clay concentration was instead calculated using TGA to be 77 wt% for PEI_{10}/MMT_{10} and 80 wt% for PEI_{10}/MMT_4. These values are extremely high relative to conventional clay-filled composites.[155] There is an increase in concentration due to additional clay being added every deposition step as the pH of the clay solution is reduced due to the PEI-covered surface being highly charged. This difference is somewhat diminished by additional PEI being deposited for the lower pH system. In an effort to demonstrate the full extent of this pH change on clay deposition, the amount of clay added per bilayer was calculated to increase from 0.42 to 0.79 $\mu g/cm^2$, almost doubling the amount of clay added per bilayer simply by lowering the pH of the clay solution. This was calculated by multiplying the average mass per bilayer obtained with the QCM by the clay mass fraction from TGA.

This high level of clay loading for the various films can be seen in TEM cross-sectional images, shown in Figure 26. For MMT at pH 10 (Figure 26(a)), there are areas of highly ordered clay platelets and also areas with gaps in the clay. In contrast, the PEI_{10}/MMT_4 film (Figure 26(b)) shows a very well-ordered structure in the majority of the thin film. The PEI_{10}/MMT_3 film is also well-ordered (Figure 26(c)), but there are areas of misalignment within the tightly packed structure, potentially from a small amount of edge-to-face bonding among the MMT platelets. This interaction occurs readily with indifferent electrolytes (such as NaCl) in solution below pH 6.5 (below this pH the edges are positively charged).[154] The indifferent electrolytes promote edge-to-face bonding by shielding opposing basal charges, but it is conceivable that some edge-to-face bonding may occur in the highly confined packing of this film. At pH 3, the clay platelet edges

have a higher positive charge and can be attracted to the negatively charged face of the deposited MMT. The AFM surface roughness values (R_q) are similar for clay pH values of 4, 8, and 10 (~30 nm), but roughness triples (to 85 nm) for PEI_{10}/MMT_3, agreeing with the waviness observed in TEM micrographs (Figure 26(c)). AFM topography of the pH 10 (Figure 27(a,b)) and pH 3 (Figure 27(d,e)) films shows the lower pH film to be much rougher at a scan size of 20 μm, but at a smaller scan size of 500 nm the features are similar, and the surfaces appears smooth without visible platelet edges. The phase images highlight the cobblestone path structure of the top layer, with many platelets visible in the 100-200 nm range (Figure 27(c,f)). Uninterrupted platelets as large as 800 nm were observed in the pH 3 system using a larger scan size (see Supporting Information). These larger platelets may have been a factor in creating a rougher film.

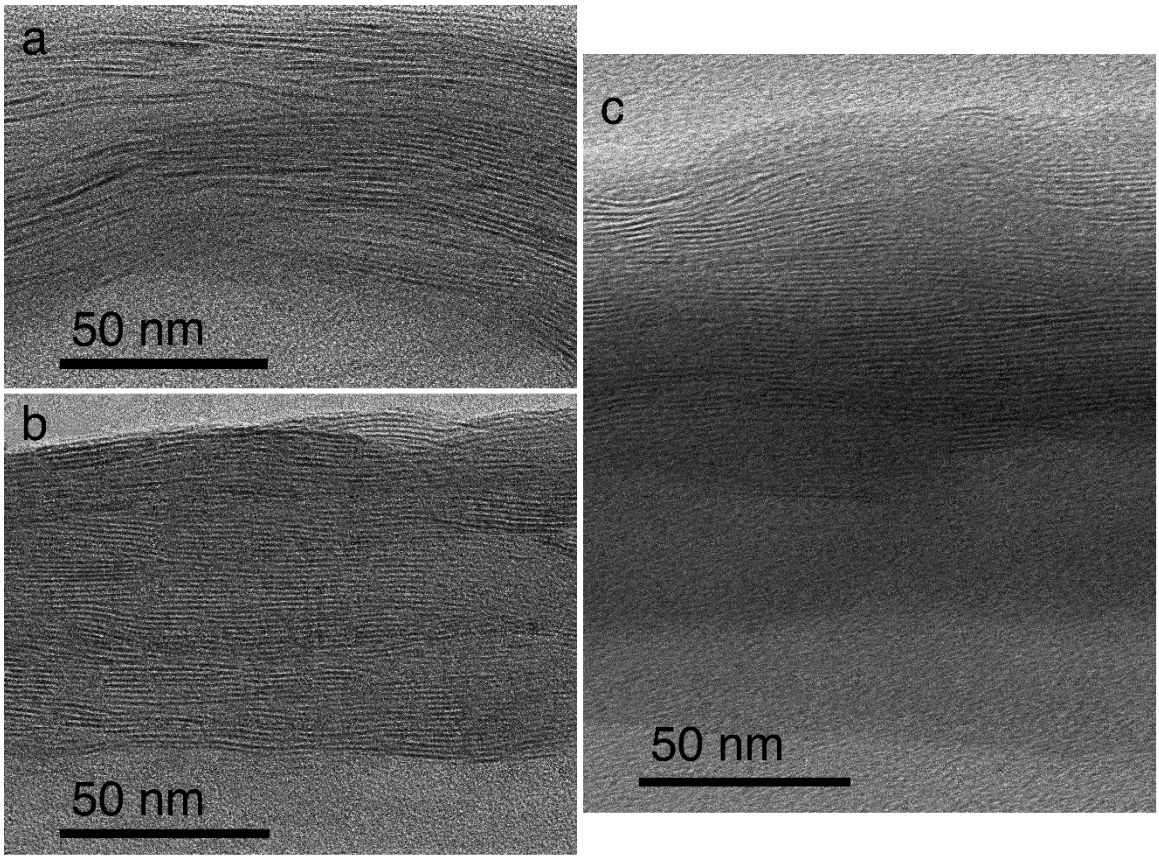

Figure 26. TEM micrographs of 10 BL (a) PEI_{10}/MMT_{10}, (b) PEI_{10}/MMT_{4}, and (c) PEI_{10}/MMT_{3} deposited on PET film.

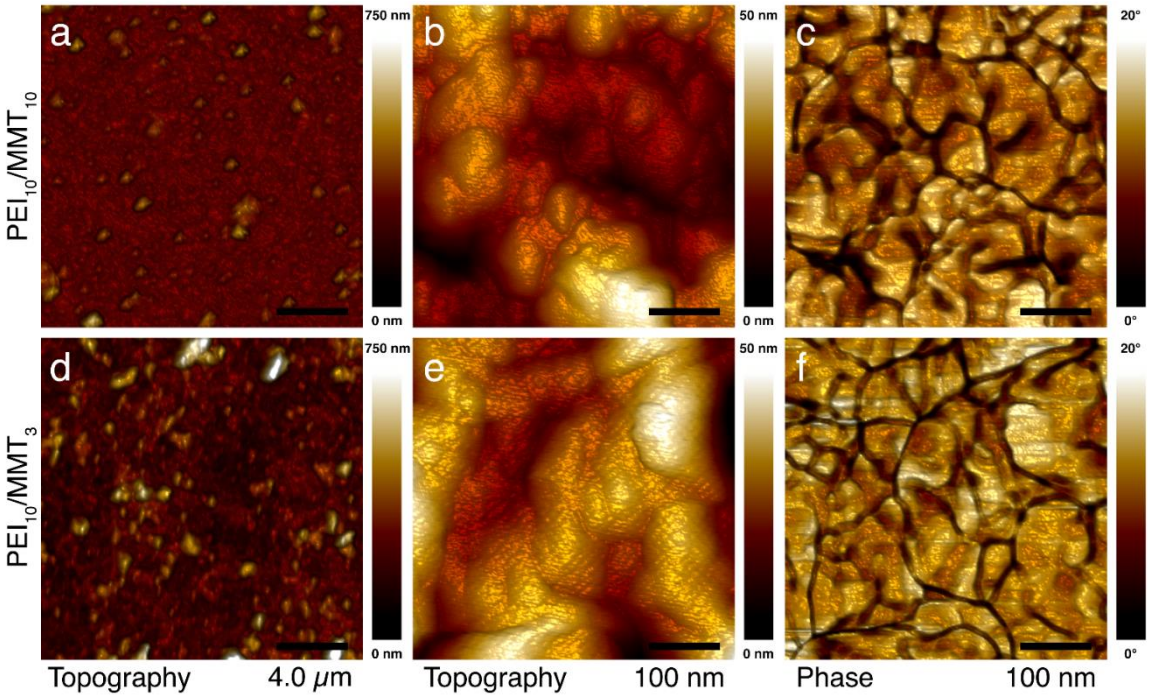

Figure 27. AFM topography (a,b,d,e) and phase images (c,f) of $[PEI_{10}/MMT_{10}]_{15}$ (top-a,b,c) and $[PEI_{10}/MMT_3]_{15}$ (bottom-d,e,f). The phase images highlight the cobblestone path structure of the MMT-covered surface and correspond to the adjacent topography (i.e., height) images (b,e).

5.3.2 Oxygen Permeability of Thin Films

Figure 28 shows oxygen transmission rate as a function of PEI_{10}/MMT_x bilayers deposited. For PEI_{10}/MMT_8, there is no improvement over PEI_{10}/MMT_{10} beyond 5 BL. At pH 4, there is more than a 5× improvement in OTR relative to the film prepared with pH 10 at 5 and 10 BL. The effective permeability (calculated using a previously described method)[89] of the $[PEI_{10}/MMT_4]_{10}$ film is $2.9\times10^{-20}\cdot cm^3\cdot cm/(cm^2\cdot s\cdot Pa)$, which is less than half the permeability reported for vapor deposited SiO_x coatings.[58] $[PEI_{10}/MMT_4]_{15}$ has an OTR of 0.09 $cm^3/(m^2\cdot day\cdot atm)$ that is two orders of magnitude lower than the bare

PET substrate that is three orders of magnitude thicker. This level of oxygen barrier approaches that of PEI/vermiculite (VMT) bilayers reported previously.[135] VMT is a clay platelet that has an aspect ratio approximately one order of magnitude larger than MMT. Larger aspect ratio clay creates a more tortuous pathway for gas molecules through the film, creating a lower transmission rate. By reducing the pH of the MMT solution, deposited layers behave as though there is a much greater effective aspect ratio (similar to skewed stacks observed in composites exposed to shear stress).[156] The pH 3 system shows improved performance at 5 BL, but is a poorer barrier than PEI_{10}/MMT_{10} at 10 and 15 BL. This is probably due to the large amount of material deposited quickly at low clay pH, but the reduced order diminishes the effectiveness of the tortuous path at 10 and 15 BL. Alignment of the clay platelets is crucial for high barrier films because they cause oxygen molecules to spend more time traveling laterally through the film rather than through the thickness.

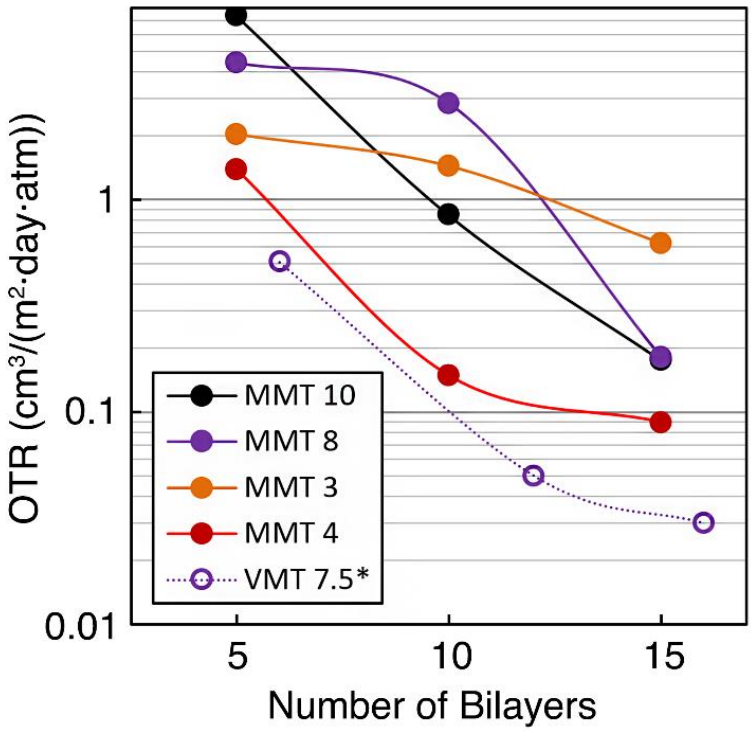

Figure 28. Oxygen transmission rate as a function of $PEI_{10}/clay_y$ bilayers deposited at varying pH (y denotes MMT suspension pH). Lines are only meant as a guide. *The data set with open circles represents PEI deposited with vermiculite clay from Reference.[135]

5.4 Conclusions

Polymer nanocomposite thin film oxygen barriers were deposited with the LbL process as a foil or SiO_x replacement. Depositing polyethylenimine from pH 10 solution and montmorillonite clay from varying pH suspensions, it was shown that the density of clay layers, and ultimately gas barrier, was altered. By reducing the pH of the clay suspension, the PEI surface became highly charged, producing a greater, more ordered deposition of MMT clay platelets. A 10 BL film deposited with pH 4 MMT provided a 5× improvement in oxygen transmission rate over the same film prepared with pH 10 clay and two orders of magnitude improvement over the 179 µm PET substrate. This pH 4

performance is comparable to that of a similar number of bilayers prepared with vermiculite clay,[35] which has an aspect ratio approximately 10× greater. At pH < 4, higher positive charge on the clay platelet edges leads to some disorder in clay orientation, and barrier is degraded. This ability to increase the effective clay aspect ratio with pH provides a means to achieve high gas barrier with lower-cost, easier-to-process clays. These water-based nanocoatings could be used to improve the performance of plastic film used for food, pharmaceutical and electronics packaging.

CHAPTER VI

CONCLUSIONS AND FUTURE WORK

6.1 Improvements on Gas Barrier Thin Films

There have been a number of improvements made to gas barrier layer-by-layer systems in this dissertation. These improvements can be applied to any LbL assembly (where nanoparticles or exponential growth are involved) to speed up the deposition process, improve the order and packing of a film, or to increase the deposition of a pH indifferent species by altering the pH. These improvements can be generalized to other systems, combined, and expanded upon. An overview of the findings and suggestions for future work are provided here.

6.1.1 Shift-Time Assembly

It was shown in Chapter III that in the PEI/PAA bilayer system, short deposition time (1 s) leads to globular deposition of polymer chains with little diffusion into the underlying polymers and a constant linear growth rate is achieved after only a few bilayers.[34] Longer dip time (i.e. 1 min) allows for relaxation of the chains in the first few depositions and diffusion in the later depositions. The film has a low initial growth rate, goes through an exponential transition, and then has a very high growth rate due to the diffusion of polymers into the underlying film. By combining the highest growth rates of the short and long deposition times, one-second exposures for the first 4 BL and one-minute for subsequent dips, a thicker and less permeable film is created. Eight bilayers (650 nm) were required to achieve an undetectable oxygen transmission rate (<0.005

$cm^3/(m^2 \cdot day)$) using one-minute deposition steps, but this barrier was obtained with only 6 BL (552 nm) using one-second deposition of the initial layers, reducing total deposition time by 73%. This "shift-time" concept makes layer-by-layer assembly much faster and more commercially feasible.

6.1.2 Similarly Charged Multilayers

The PEI/MMT system has been shown to impart significant barrier to polymer substrates in the past.[11, 92] In Chapter IV this system was improved upon by introducing a PAA deposition after each MMT deposition, which effectively filled in the gaps between the deposited clay platelets.[141] This PEI/MMT/PAA trilayer system has a smoother surface and greatly decreased permeability to oxygen when compared to a similar number of PEI/MMT bilayers. The oxygen transmission rate was reduced by an order of magnitude with 10 clay layers.

6.1.3 Altering Clay-pH

An alternative method of improving the performance of the PEI/MMT system was explored in Chapter V. The amount of clay deposited every cycle was approximately doubled by simply altering the pH of the clay suspension,[38] despite the charge of montmorillonite not being highly dependent upon pH. It was observed that the bilayer system grows extremely thickly at pH 3, but the resulting film is not highly ordered and the oxygen barrier suffers accordingly. The PEI/MMT_4 bilayer system performs almost an order of magnitude better than the PEI/MMT_{10} system at the same number of bilayers, almost as good of a barrier as a film with clay platelets with an aspect ratio an order of magnitude larger.

6.2 Future Research Direction

6.2.1 Clay pH Quadlayer

It has been shown previously that including additional polymer layers between clay layers can decrease the permeability of the thin film by providing more volume for the gas particles to reside in before accessing a gap in the clay layer.[12, 157] As demonstrated in Chapter V, reducing the pH of the clay suspension in the PEI/MMT system increases the clay deposition, improving the oxygen barrier performance. Optimizing the pH of the MMT suspension for the PEI/PAA/PEI/MMT quadlayer system is not as straightforward as using the optimized clay pH for the BL system. The QL system's growth behavior is due to a diffusion of the polymers through the clay layer, which leads to exponential growth at pH 10.[35] As pH of MMT is decreased, additional clay is deposited that suppresses exponential growth, as shown in Figure 29(a). This leads to a tradeoff between thick clay deposition and polymer diffusion (leading to thicker growth), shown schematically in Figure 29(b), which are two methods of reducing permeability.

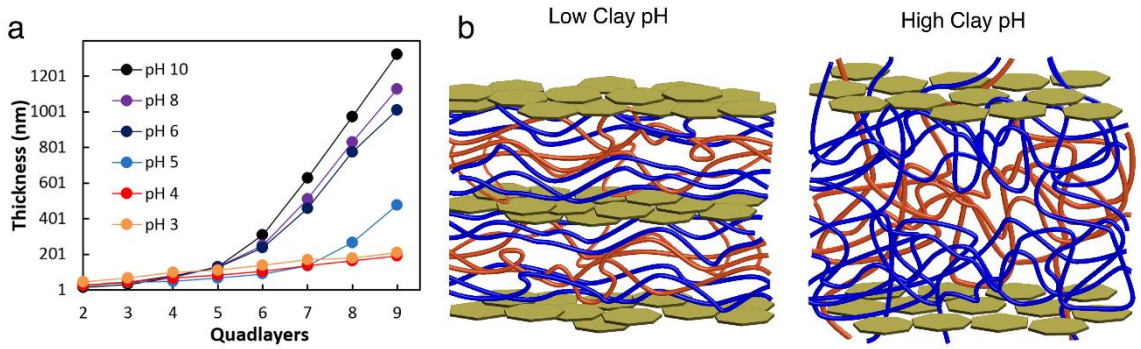

Figure 29. (a) Thickness of PEI/PAA/PEI/MMT QL with the MMT deposited at varying pH. PEI and PAA depositions were held at constant pH 10 and 4, respectively. (b) Schematic of deposition with low and high clay pH.

TEM cross-sectional images confirm that 5 QL of MMT at pH 10 is thicker, but has a more open structure than the QL constructed with MMT at pH 4 (Figure 30 (b) and (a), respectively). The minimum OTR of the pH's tested in the range between 4 and 10 occurs at pH 5 and 6, as shown in Figure 31. The pH 5 system reaches an undetectable OTR level (0.005 $cm^3/(m^2 \cdot day)$) at 3 QL, while pH 6 is below this level. MMT at pH 3 shows the least improvement in barrier due to the high level of disorder of the MMT, as described in Chapter V.

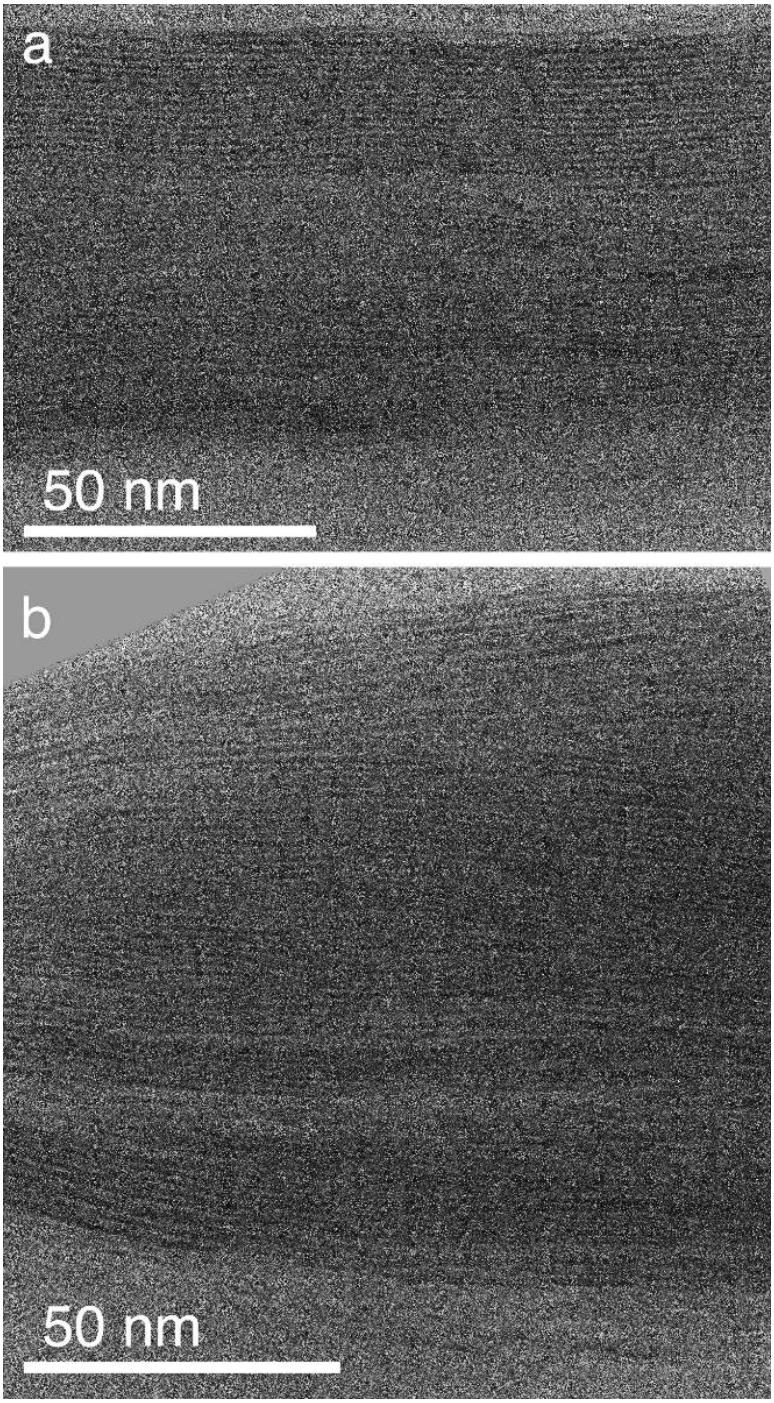

Figure 30. Transmission electron micrographs of 5 QL's PEI/PAA/PEI/MMT with MMT at (a) pH 4 and (b) pH 10.

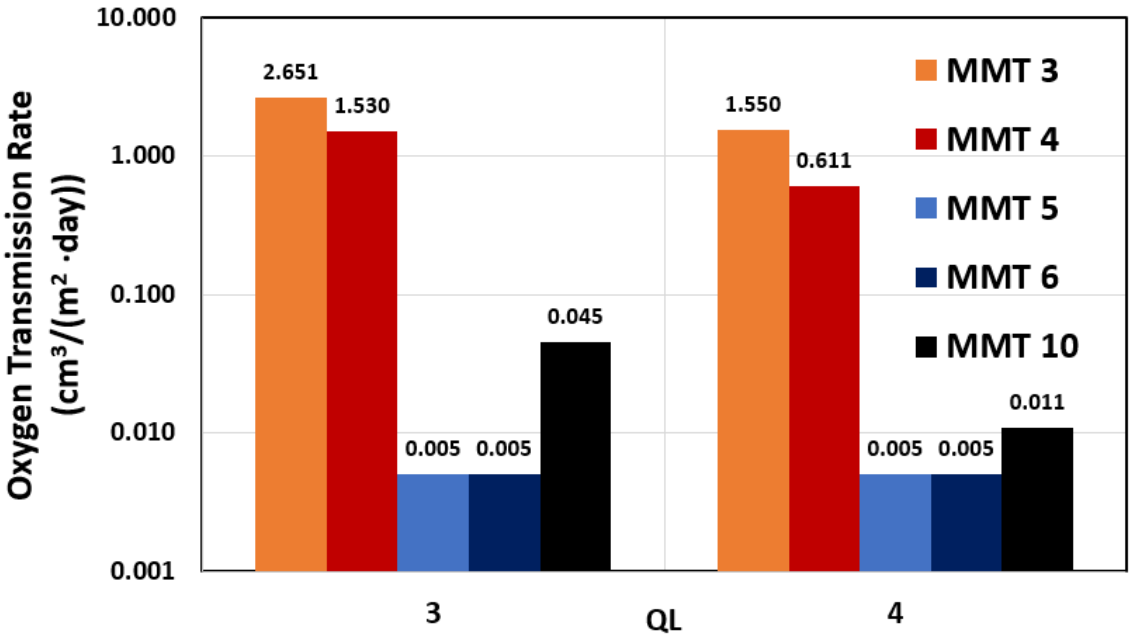

Figure 31. Oxygen transmission rate of PEI/PAA/PEI/MMT QL systems, with MMT deposited at varying pH.

6.2.2 Combined Deposition Time and Clay pH Studies

The methods of improving barrier discussed in Chapters III, IV, and Section 6.2.1 can be combined to further improve gas barrier for a given number of layers. It has been shown previously that reducing the deposition time of PEI does not impair the gas barrier properties of the resulting film, while reducing the clay deposition time does.[109] Beginning with the time-dependent deposition behavior of PEI and PAA presented in Chapter III, the influence of polymer deposition time can be examined in conjunction with the extent of diffusion of depositing polymer through the previously deposited clay layer. As a proof of concept, 3 QL of PEI/PAA/PEI/ MMT_4 (where little polymer diffusion is expected due to the high level of clay deposited) were deposited with 1 second polymer

depositions and 1 min clay depositions, which resulted in an oxygen transmission rate of 0.22165 $cm^3/(m^2 \cdot day \cdot atm)$. This is an 85% reduction relative to the same film with 1 minute polymer depositions. Whether or not the barrier will be improved at pH 5 and 6 remains to be seen, as the exponential growth will most likely be hindered due to reduced time for diffusion of polymer through the clay layer. This result can be greatly expanded upon by varying pH of the clay and the length of various polymer depositions individually.

6.2.3 Edge Charge Neutralization

Chapters IV and V both examined ways to bolster the clay layer in the PEI/MMT system, either by adding a polymer to fill in gaps in the clay coverage or depositing more clay, in an effort to improve oxygen barrier properties. A third approach would be to cause the clay platelets to join at the edges rather than to allow random deposition. It has been shown that in solution, MMT platelets exhibit edge-to-edge bonding in the presence of salt at pH 6.5. At pH 6.5 the amphoteric edge sites have a neutral net charge and sufficient salt will effectively shield the charge from neighboring platelets, allowing van der Waals forces to attract the edges to one another.[154] The edges become positively charged below this pH and can actually exhibit edge-to-face bonding, forming a "house of cards" structure, as shown in Figure 32. This type of formation would not be favorable for barrier films, but could potentially reduce film density (and lower refractive index). If MMT is deposited from a pH 6.5 suspension with salt, it is possible to deposit with better clay coverage, creating a more tortuous path for diffusing gas particles. The charge screening effect of the salt could also work against the formation of the thin film, possibly screening

the attraction between the deposited PEI and clay platelets in suspension, this needs to be explored.

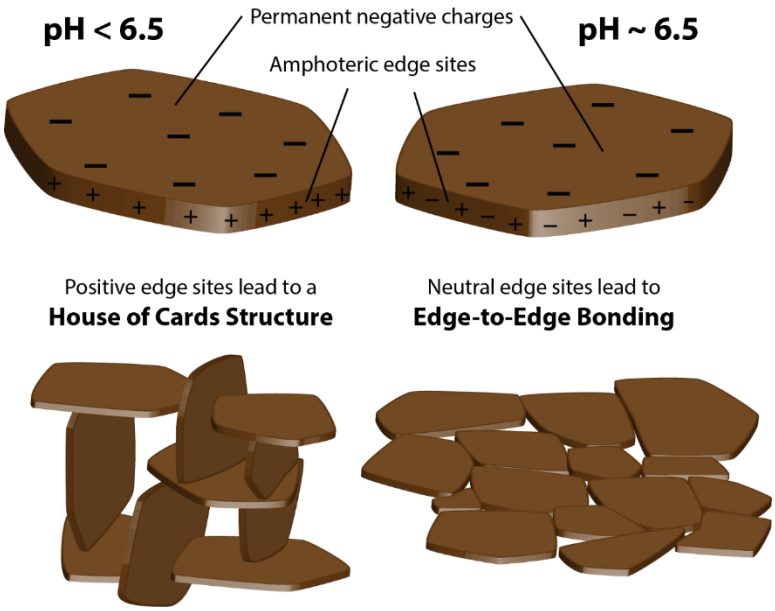

Figure 32. Illustration of MMT formations in suspensions at and below pH 6.5 in the presence of salt.

As a proof of concept 8 BL of PEI/MMT was deposited onto PET with the MMT suspension at pH 6.5. Two different films were made, one with 10 mmol NaCl and one with 100 mmmol NaCl. The resulting oxygen transmission rates were 0.35 and 1.75, respectively. The 8 BL film prepared with 10 mmol NaCl cut the OTR in half relative to a **10 BL** film made without salt. A 3 QL film prepared with 100mmol NaCl did not show improvement over the 3 QL film at pH 5, described in Section 6.2.1, but a lower number of quadlayers should be investigated with a lower salt concentration.

6.2.4 Demonstrate the Scalability of the LbL Dipping Process

Figure 33 shows a pilot scale LbL dipping apparatus has been constructed with the ability to coat quadlayer films with dip rinsing and air knife drying. The performance of films cut from a 50-foot web coated with this machine should be evaluated and compared to those made with the traditional dipping process. The work performed in this dissertation should lay the groundwork for optimizing the continuous process as deposition time will be a variable that will be influenced by the line speed. Preliminary results from the robot dipping process has shown that rinsing and/or drying may be eliminated without compromising the oxygen barrier performance of the film. Initial runs of the continuous dipping apparatus has shown barrier performance comparable to (or exceeding) those obtained in the batch dipping process.

Figure 33. Schematic (left) and picture (right) of pilot scale continuous LbL coating apparatus.

REFERENCES

1. Graff, G. L.; Burrows, P. E.; Williford, R. E.; Praino, R. F. Barrier Layer Technology for Flexible Displays. In *Flexible Flat Panel Displays*; John Wiley & Sons, Ltd: Chichester, UK, 2005, pp 57-77.

2. Bowles, M.; Jianjun, L. In *Review on Nanotechnology in Agricultural Products Logistics Management*, 8th International Conference on Computing and Networking Technology (ICCNT), 27-29 Aug. 2012; 2012, pp 415-420.

3. Yam, K. L.; Lee, D. S. *Emerging Food Packaging Technologies: Principles and Practice*; Woodhead Publishing: Cambridge, UK, 2012.

4. Das, S.; Yin, W. Trends in the Global Aluminum Fabrication Industry. *JOM* **2007,** *59* (2), 83-87.

5. Leterrier, Y. Durability of Nanosized Oxygen-Barrier Coatings on Polymers. *Prog. Mater Sci.* **2003,** *48* (1), 1-55.

6. Affinito, J. D.; Gross, M. E.; Coronado, C. A.; Graff, G. L.; Greenwell, E. N.; Martin, P. M. A New Method for Fabricating Transparent Barrier Layers. *Thin Solid Films* **1996,** *290*, 63-67.

7. Zehetmeyer, G.; Scheibel, J. M.; Soares, R. M. D.; Weibel, D. E.; Oviedo, M. A. S.; Oliveira, R. V. B. Morphological, Optical, and Barrier Properties of PP/MMT Nanocomposites. *Polym. Bull.* **2013,** *70* (8), 2181-2191.

8. Hayrapetyan, S.; Kelarakis, A.; Estevez, L.; Lin, Q.; Dana, K.; Chung, Y.-L.; Giannelis, E. P. Non-Toxic Poly(ethylene terephthalate)/Clay Nanocomposites with Enhanced Barrier Properties. *Polymer* **2012,** *53* (2), 422-426.

9. Nazarenko, S.; Meneghetti, P.; Julmon, P.; Olson, B. G.; Qutubuddin, S. Gas Barrier of Polystyrene Montmorillonite Clay Nanocomposites: Effect of Mineral Layer Aggregation. *J. Polym. Sci., Part B: Polym. Phys.* **2007,** *45* (13), 1733-1753.

10. Decher, G.; Schlenoff, J. B. *Multilayer Thin Films*; Wiley-VCH Verlag GmbH & Co. KGaA Weinheim, Germany, 2012.

11. Priolo, M. A.; Gamboa, D.; Grunlan, J. C. Transparent Clay−Polymer Nano Brick Wall Assemblies with Tailorable Oxygen Barrier. *ACS Appl. Mater. Interfaces* **2010,** *2* (1), 312-320.

12. Priolo, M. A.; Gamboa, D.; Holder, K. M.; Grunlan, J. C. Super Gas Barrier of Transparent Polymer−Clay Multilayer Ultrathin Films. *Nano Lett.* **2010,** *10* (12), 4970-4974.

13. Svagan, A. J.; Åkesson, A.; Cárdenas, M.; Bulut, S.; Knudsen, J. C.; Risbo, J.; Plackett, D. Transparent Films Based on PLA and Montmorillonite with Tunable Oxygen Barrier Properties. *Biomacromolecules* **2012,** *13* (2), 397-405.

14. Ratanatawanate, C.; Perez, M.; Gnade, B. E.; Balkus Jr, K. J. Layer-by-Layer Assembly of Titanate Nanosheets/Poly-(ethylenimine) on PEN Films. *Mater. Lett.* **2012,** *66* (1), 242-245.

15. Yang, Y.-H.; Haile, M.; Park, Y. T.; Malek, F. A.; Grunlan, J. C. Super Gas Barrier of All-Polymer Multilayer Thin Films. *Macromolecules* **2011,** *44* (6), 1450-1459.

16. Yang, Y.-H.; Bolling, L.; Priolo, M. A.; Grunlan, J. C. Super Gas Barrier and Selectivity of Graphene Oxide-Polymer Multilayer Thin Films. *Adv. Mater.* **2013,** *25* (4), 503-508.

17. Gilbert, J. B.; O'Brien, J. S.; Suresh, H. S.; Cohen, R. E.; Rubner, M. F. Orientation-Specific Attachment of Polymeric Microtubes on Cell Surfaces. *Adv. Mater.* **2013,** *25* (41), 5974-5952.

18. Hong, J.; Alvarez, L.; Shah, N.; Cho, Y.; Kim, B.-S.; Griffith, L.; Char, K.; Hammond, P. Multilayer Thin-Film Coatings Capable of Extended Programmable Drug Release: Application to Human Mesenchymal Stem Cell Differentiation. *Drug Delivery and Translational Research* **2012,** *2* (5), 375-383.

19. Cui, J.; Yan, Y.; Wang, Y.; Caruso, F. Drug Delivery: Templated Assembly of pH-Labile Polymer-Drug Particles for Intracellular Drug Delivery (Adv. Funct. Mater. 22/2012). *Adv. Funct. Mater.* **2012,** *22* (22), 4844-4844.

20. Zhai, L.; Cebeci, F. C.; Cohen, R. E.; Rubner, M. F. Stable Superhydrophobic Coatings from Polyelectrolyte Multilayers. *Nano Lett.* **2004,** *4* (7), 1349-1353.

21. Zhang, L.; Sun, J. Q. Layer-by-Layer Codeposition of Polyelectrolyte Complexes and Free Polyelectrolytes for the Fabrication of Polymeric Coatings. *Macromolecules* **2010,** *43* (5), 2413-2420.

22. Lichter, J. A.; Van Vliet, K. J.; Rubner, M. F. Design of Antibacterial Surfaces and Interfaces: Polyelectrolyte Multilayers as a Multifunctional Platform. *Macromolecules* **2009,** *42* (22), 8573-8586.

23. Laufer, G.; Kirkland, C.; Morgan, A. B.; Grunlan, J. C. Exceptionally Flame Retardant Sulfur-Based Multilayer Nanocoating for Polyurethane Prepared from Aqueous Polyelectrolyte Solutions. *ACS Macro Lett.* **2013,** *2* (5), 361-365.

24. Cain, A. A.; Nolen, C. R.; Li, Y.-C.; Davis, R.; Grunlan, J. C. Phosphorous-Filled Nanobrick Wall Multilayer Thin Film Eliminates Polyurethane Melt Dripping and Reduces Heat Release Associated with Fire. *Polym. Degrad. Stab.* **2013,** *98* (12), 2645-2652.

25. Shim, B. S.; Zhu, J. A.; Jan, E.; Critchley, K.; Kotov, N. A. Transparent Conductors from Layer-by-Layer Assembled SWNT Films: Importance of Mechanical Properties and a New Figure of Merit. *ACS Nano* **2010,** *4* (7), 3725-3734.

26. Huang, C.; Grobert, N.; Watt, A. A. R.; Johnston, C.; Crossley, A.; Young, N. P.; Grant, P. S. Layer-by-Layer Spray Deposition and Unzipping of Single-Wall Carbon Nanotube-Based Thin Film Electrodes for Electrochemical Capacitors. *Carbon* **2013,** *61* (0), 525-536.

27. Kharlampieva, E.; Kozlovskaya, V.; Sukhishvili, S. A. Layer-by-Layer Hydrogen-Bonded Polymer Films: From Fundamentals to Applications. *Adv. Mater.* **2009,** *21* (30), 3053-3065.

28. Kekicheff, P.; Schneider, G. F.; Decher, G. Size-Controlled Polyelectrolyte Complexes: Direct Measurement of the Balance of Forces Involved in the Triggered Collapse of Layer-by-Layer Assembled Nanocapsules. *Langmuir* **2013,** *29* (34), 10713-10726.

29. Kharlampieva, E.; Kozlovskaya, V.; Zavgorodnya, O.; Lilly, G. D.; Kotov, N. A.; Tsukruk, V. V. pH-Responsive Photoluminescent LbL Hydrogels with Confined Quantum Dots. *Soft Matter* **2010,** *6* (4), 800-807.

30. Boudou, T.; Crouzier, T.; Nicolas, C.; Ren, K.; Picart, C. Polyelectrolyte Multilayer Nanofilms Used as Thin Materials for Cell Mechano-Sensitivity Studies. *Macromol. Biosci.* **2011,** *11* (1), 77-89.

31. Nestler, P.; Paßvogel, M.; Helm, C. A. Influence of Polymer Molecular Weight on the Parabolic and Linear Growth Regime of PDADMAC/PSS Multilayers. *Macromolecules* **2013,** *46* (14), 5622-5629.

32. Sui, Z. J.; Salloum, D.; Schlenoff, J. B. Effect of Molecular Weight on the Construction of Polyelectrolyte Multilayers: Stripping Versus Sticking. *Langmuir* **2003,** *19* (6), 2491-2495.

33. Porcel, C.; Lavalle, P.; Decher, G.; Senger, B.; Voegel, J. C.; Schaaf, P. Influence of the Polyelectrolyte Molecular Weight on Exponentially Growing Multilayer Films in the Linear Regime. *Langmuir* **2007,** *23* (4), 1898-1904.

34. Hagen, D. A.; Foster, B.; Stevens, B.; Grunlan, J. C. Shift-Time Polyelectrolyte Multilayer Assembly: Fast Film Growth and High Gas Barrier with Fewer Layers by Adjusting Deposition Time. *ACS Macro Lett.* **2014,** *3* (7), 663-666.

35. Podsiadlo, P.; Michel, M.; Lee, J.; Verploegen, E.; Kam, N. W. S.; Ball, V.; Lee, J.; Qi, Y.; Hart, A. J.; Hammond, P. T.; Kotov, N. A. Exponential Growth of LBL Films with Incorporated Inorganic Sheets. *Nano Lett.* **2008,** *8* (6), 1762-1770.

36. Bieker, P.; Schönhoff, M. Linear and Exponential Growth Regimes of Multilayers of Weak Polyelectrolytes in Dependence on pH. *Macromolecules* **2010,** *43* (11), 5052-5059.

37. Fernandez, R.; Ocando, C.; Fernandes, S. C. M.; Eceiza, A.; Tercjak, A. Optically Active Multilayer Films Based on Chitosan and an Azopolymer. *Biomacromolecules* **2014,** *15* (4), 1399-1407.

38. Hagen, D. A.; Saucier, L.; Grunlan, J. C. Controlling Effective Aspect Ratio and Packing of Clay with pH for Improved Gas Barrier in Nanobrick Wall Thin Films. *ACS Appl. Mater. Interfaces* **2014,** *6* (24), 22914-22919.

39. Tzeng, P.; Maupin, C. R.; Grunlan, J. C. Influence of Polymer Interdiffusion and Clay Concentration on Gas Barrier of Polyelectrolyte/Clay Nanobrick Wall Quadlayer Assemblies. *J. Membr. Sci.* **2014,** *452* (0), 46-53.

40. Ferreira, M.; Rubner, M. F. Molecular-Level Processing of Conjugated Polymers .1. Layer-By-Layer Manipulation of Conjugated Polyions. *Macromolecules* **1995,** *28* (21), 7107-7114.

41. McAloney, R. A.; Sinyor, M.; Dudnik, V.; Goh, M. C. Atomic Force Microscopy Studies of Salt Effects on Polyelectrolyte Multilayer Film Morphology. *Langmuir* **2001,** *17* (21), 6655-6663.

42. Buscher, K.; Graf, K.; Ahrens, H.; Helm, C. A. Influence of Adsorption Conditions on the Structure of Polyelectrolyte Multilayers. *Langmuir* **2002,** *18* (9), 3585-3591.

43. Lu, Y.; Lu, A.; Zhuk, L.; Xu, X.; Liang, E.; Kharlampieva, S.; Sukhishvili. Tunable pH and Temperature Response of Weak Polyelectrolyte Brushes: Role of Hydrogen Bonding and Monomer Hydrophobicity. *Soft matter* **2013,** *9* (22), 5464.

44. Kamal, M.; Jinnah, I.; Utracki, L. Permeability of oxygen and water vapor through polyethylene/polyamide films. *Polymer Engineering & Science* **1984,** *24* (17), 1337-1347.

45. Charton, C.; Schiller, N.; Fahland, M.; Holländer, A.; Wedel, A.; Noller, K. Development of High Barrier Films on Flexible Polymer Substrates. *Thin Solid Films* **2006,** *502* (1–2), 99-103.

46. Lange, J.; Wyser, Y. Recent Innovations in Barrier Technologies for Plastic Packaging—a Review. *Packaging Technology and Science* **2003,** *16* (4), 149-158.

47. Willhite, C. C.; Karyakina, N. A.; Yokel, R. A.; Yenugadhati, N.; Wisniewski, T. M.; Arnold, I. M. F.; Momoli, F.; Krewski, D. Systematic Review of Potential Health Risks Posed by Pharmaceutical, Occupational and Consumer Exposures to Metallic and Nanoscale Aluminum, Aluminum Oxides, Aluminum Hydroxide and its Soluble Salts. *Crit. Rev. Toxicol.* **2014,** *44* (S4), 1-80.

48. Fukuzumi, H.; Saito, T.; Iwata, T.; Kumamoto, Y.; Isogai, A. Transparent and High Gas Barrier Films of Cellulose Nanofibers Prepared by TEMPO-Mediated Oxidation. *Biomacromolecules* **2008,** *10* (1), 162-165.

49. Mattox, D. M. Chapter 1 - Introduction. In *Handbook of Physical Vapor Deposition (PVD) Processing (Second Edition)*, Mattox, D. M., Ed.; William Andrew Publishing: Boston, 2010, pp 1-24.

50. Mattox, D. M. Chapter 6 - Vacuum Evaporation and Vacuum Deposition. In *Handbook of Physical Vapor Deposition (PVD) Processing (Second Edition)*, Mattox, D. M., Ed.; William Andrew Publishing: Boston, 2010, pp 195-235.

51. Schiller, N.; Straach, S.; Fahland, M.; Charton, C. In *Barrier coatings on plastic web*, Proceedings of the Annual Technical Conference-Society of Vacuum Coaters 2001, pp 184-188.

52. Mattox, D. M. Chapter 3 - The "Good" Vacuum (Low Pressure) Processing Environment. In *Handbook of Physical Vapor Deposition (PVD) Processing (Second Edition)*, Mattox, D. M., Ed.; William Andrew Publishing: Boston, 2010, pp 73-145.

53. Plichta, A.; Habeck, A.; Knoche, S.; Kruse, A.; Weber, A.; Hildebrand, N. Flexible Glass Substrates. In *Flexible Flat Panel Displays*; John Wiley & Sons, Ltd, 2005, pp 35-55.

54. Masuda, A.; Umemoto, H.; Matsumura, H. Various Applications of Silicon Nitride by Catalytic Chemical Vapor Deposition for Coating, Passivation and Insulating Films. *Thin Solid Films* **2006,** *501* (1–2), 149-153.

55. Matsumura, H. Low Temperature Deposition of Silicon Nitride by the Catalytic Chemical Vapor Deposition Method. *Jpn. J. Appl. Phys.* **1989,** *28* (10R), 2157.

56. George, S. M. Atomic Layer Deposition: An Overview. *Chem. Rev.* **2009,** *110* (1), 111-131.

57. Struller, C.; Kelly, P.; Copeland, N.; Tobin, V.; Assender, H.; Holliday, C.; Read, S. Aluminium Oxide Barrier Films on Polymeric Web and Their Conversion for Packaging Applications. *Thin Solid Films* **2014,** *553*, 153-156.

58. Roberts, A.; Henry, B.; Sutton, A.; Grovenor, C.; Briggs, G.; Miyamoto, T.; Kano, M.; Tsukahara, Y.; Yanaka, M. Gas Permeation in Silicon-Oxide/Polymer (Siox/Pet) Barrier Films: Role of the Oxide Lattice, Nano-Defects and Macro-Defects. *J. Membr. Sci.* **2002,** *208* (1), 75-88.

59. Inagaki, N.; Tasaka, S.; Hiramatsu, H. Preparation Of Oxygen Gas Barrier Poly (Ethylene Terephthalate) Films By Deposition Of Silicon Oxide Films Plasma-Polymerized from a Mixture of Tetramethoxysilane and Oxygen. *J. Appl. Polym. Sci.* **1999,** *71* (12), 2091-2100.

60. Sinha Ray, S.; Okamoto, M. Polymer/Layered Silicate Nanocomposites: A Review from Preparation to Processing. *Prog. Polym. Sci.* **2003,** *28* (11), 1539-1641.

61. Jordan, J.; Jacob, K. I.; Tannenbaum, R.; Sharaf, M. A.; Jasiuk, I. Experimental Trends in Polymer Nanocomposites—a Review. *Materials Science and Engineering: A* **2005,** *393* (1–2), 1-11.

62. Hussain, F.; Hojjati, M.; Okamoto, M.; Gorga, R. E. Review article: Polymer-matrix Nanocomposites, Processing, Manufacturing, and Application: An Overview. *J. Compos. Mater.* **2006,** *40* (17), 1511-1575.

63. Pavlidou, S.; Papaspyrides, C. D. A Review on Polymer–Layered Silicate Nanocomposites. *Prog. Polym. Sci.* **2008,** *33* (12), 1119-1198.

64. Faucheu, J.; Gauthier, C.; Chazeau, L.; Cavaillé, J.-Y.; Mellon, V.; Lami, E. B. Miniemulsion Polymerization for Synthesis of Structured Clay/Polymer Nanocomposites: Short Review and Recent Advances. *Polymer* **2010,** *51* (1), 6-17.

65. Calebrese, C.; Le, H.; Schadler, L. S.; Nelson, J. K. A Review on the Importance of Nanocomposite Processing to Enhance Electrical Insulation. *Dielectrics and Electrical Insulation, IEEE Transactions on* **2011,** *18* (4), 938-945.

66. Kango, S.; Kalia, S.; Celli, A.; Njuguna, J.; Habibi, Y.; Kumar, R. Surface Modification of Inorganic Nanoparticles for Development of Organic–Inorganic Nanocomposites—A review. *Prog. Polym. Sci.* **2013,** *38* (8), 1232-1261.

67. Lin, F. Preparation and Characterization of Polymer Tio_2 Nanocomposites Via In-Situ Polymerization. University of Waterloo2006.

68. Ghezelbash, Z.; Ashouri, D.; Mousavian, S.; Ghandi, A. H.; Rahnama, Y. Surface Modified Al_2O_3 in Fluorinated Polyimide/Al_2O_3 Nanocomposites: Synthesis and Characterization. *Bull. Mater. Sci.* **2012,** *35* (6), 925-931.

69. Guo, B.; Zhao, Y.; Liu, H.; Huang, Y.; Feng, T.; Jiao, Q. Preparation of UV-Curable Nanocomposite Varnish with High Wear Resistance. 2012;229, 121-125.

70. Mueller, P.; Woerner, C.; Schaefer, R.; Muelhaupt, R. In *Organosilicon 1,3-Oxazolines: Reactive Silicone Liquid Rubbers and Silane Coupling Agents Tailored for Reactive Processing Application and Nanocomposite Formation*, 1997, 51-52.

71. Nakamura, Y.; Nagata, K.; Tobita, Y.; Yokouchi, N.; Nigo, H.; Iida, T. Surface Structure Of Silane-Treated Glass Beads And Its Influence on the Mechanical Properties Of Filled Composites. *J. Adhes. Sci. Technol.* **2002,** *16* (5), 523-542.

72. Stojanovič, S.; Bauer, F.; Gläsel, H. J.; Mehnert, R. Scratch and Abrasion Resistant Polymeric Nanocomposites - Preparation, Characterization and Applications. 2004; Vol. 453-454, pp 473-478.

73. Sun, Y.; Zhang, Z.; Wong, C. P. In *Influence of Nanosilica on Composite Underfill Properties In Flip Chip Packaging*, 2004, 253-259.

74. Vuluga, Z.; Donescu, D.; Radovici, C.; Şerban, S.; Paven, H. Coupling and Compatibilizer Agents Effects in Polystyrene/Layered Silicate Nanocomposites. *UPB Scientific Bulletin, Series B: Chemistry and Materials Science* **2004,** *66* (1), 33-42.

75. Sideridou, I. D.; Karabela, M. M. Effect of the Structure of Silane-Coupling Agent on Dynamic Mechanical Properties of Dental Resin-Nanocomposites. *J. Appl. Polym. Sci.* **2008,** *110* (1), 507-516.

76. Wang, C.; Mao, H.; Wang, C.; Fu, S. Dispersibility and Hydrophobicity Analysis of Titanium Dioxide Nanoparticles Grafted with Silane Coupling Agent. *Ind. Eng. Chem. Res.* **2011,** *50* (21), 11930-11934.

77. Truong, L. T.; Larsen, Å.; Holme, B.; Diplas, S.; Hansen, F. K.; Roots, J.; Jørgensen, S. Dispersibility of Silane-Functionalized Alumina Nanoparticles in Syndiotactic Polypropylene. *Surf. Interface Anal.* **2010,** *42* (6-7), 1046-1049.

78. Rong, M. Z.; Zhang, M. Q.; Zheng, Y. X.; Zeng, H. M.; Walter, R.; Friedrich, K. Structure–Property Relationships of Irradiation Grafted Nano-Inorganic Particle Filled Polypropylene Composites. *Polymer* **2001,** *42* (1), 167-183.

79. Sato, K.; Kondo, S.; Tsukada, M.; Ishigaki, T.; Kamiya, H. Influence of Solid Fraction on the Optimum Molecular Weight of Polymer Dispersants in Aqueous TiO2 Nanoparticle Suspensions. *J. Am. Ceram. Soc.* **2007,** *90* (11), 3401-3406.

80. Ling Hu, A. P., Denis Chaumont and Claire-Helene Brachais. *Microwave Synthesis Of Core-Shell Structured Biocompatible Magnetic Nanohybrids in Aqueous Medium* 2011.

81. Werner E. van Zyl, M. G. Hybrid Polyamide/Silica Nanocomposites: Synthesis and Mechanical Testing. *Macromolecular Materials and Engineering* **2002,** *287*, 106-110.

82. Balan, L.; Burget, D. Synthesis of Metal/Polymer Nanocomposite by Uv-Radiation Curing. *Eur. Polym. J.* **2006,** *42* (12), 3180-3189.

83. Zhou, Y.; Hao, L. Y.; Zhu, Y. R.; Hu, Y.; Chen, Z. Y. A Novel Ultraviolet Irradiation Technique for Fabrication of Polyacrylamide–metal (M = Au, Pd) Nanocomposites at Room Temperature. *J. Nanopart. Res.* **2001,** *3* (5-6), 377-381.

84. Kojima, Y.; Usuki, A.; Kawasumi, M.; Okada, A.; Fukushima, Y.; Kurauchi, T.; Kamigaito, O. Mechanical Properties of Nylon 6-Clay Hybrid. *Journal of Materials Research(USA)* **1993,** *8* (5), 1185-1189.

85. Usuki, A.; Kojima, Y.; Kawasumi, M.; Okada, A.; Fukushima, Y.; Kurauchi, T.; Kamigaito, O. Synthesis of Nylon 6-clay Hybrid. *Journal of Materials Research(USA)* **1993,** *8* (5), 1179-1184.

86. Usuki, A.; Kawasumi, M.; Kojima, Y.; Okada, A.; Kurauchi, T.; Kamigaito, O. Swelling Behavior of Montmorillonite Cation Exchanged for X-Amino Acids by E-Caprolactam. *J. Mater. Res.* **1993,** *8* (5), 1174-1178.

87. Fujimori, A. Mixed Monolayers of Biodegradable Polymers and an Organo-Modified Clay. http://www.4spepro.org/pdf/003663/003663.pdf.

88. Osman, M. A.; Mittal, V.; Morbidelli, M.; Suter, U. W. Epoxy-Layered Silicate Nanocomposites and Their Gas Permeation Properties. *Macromolecules* **2004,** *37* (19), 7250-7257.

89. Nielsen, L. E. Models for the Permeability of Filled Polymer Systems. *J. Macromol. Sci., Pure Appl. Chem.* **1967,** *1* (5), 929-942.

90. Cussler, E. L.; Hughes, S. E.; Ward Iii, W. J.; Aris, R. Barrier membranes. *J. Membr. Sci.* **1988,** *38* (2), 161-174.

91. Falla, W. R.; Mulski, M.; Cussler, E. L. Estimating Diffusion Through Flake-Filled Membranes. *J. Membr. Sci.* **1996,** *119* (1), 129-138.

92. Priolo, M. A.; Holder, K. M.; Gamboa, D.; Grunlan, J. C. Influence of Clay Concentration on the Gas Barrier of Clay–Polymer Nanobrick Wall Thin Film Assemblies. *Langmuir* **2011,** *27* (19), 12106-12114.

93. Herrera-Alonso, J. M.; Marand, E.; Little, J. C.; Cox, S. S. Transport Properties in Polyurethane/clay Nanocomposites as Barrier Materials: Effect of Processing Conditions. *J. Membr. Sci.* **2009,** *337* (1–2), 208-214.

94. Grunlan, J. C.; Grigorian, A.; Hamilton, C. B.; Mehrabi, A. R. Effect of Clay Concentration on the Oxygen Permeability and Optical Properties of a Modified Poly(vinyl alcohol). *J. Appl. Polym. Sci.* **2004,** *93* (3), 1102-1109.

95. Ebina, T.; Mizukami, F. Flexible Transparent Clay Films with Heat-Resistant and High Gas-Barrier Properties. *Adv. Mater.* **2007,** *19* (18), 2450-2453.

96. Kumar, S. A.; Yuelong, H.; Yumei, D.; Le, Y.; Kumaran, M.; Thomas, S. Gas Transport Through Nano Poly(ethylene-co-vinyl acetate) Composite Membranes. *Ind. Eng. Chem. Res.* **2008,** *47* (14), 4898-4904.

97. Gain, O.; Espuche, E.; Pollet, E.; Alexandre, M.; Dubois, P. Gas Barrier Properties of Poly(e-caprolactone)/Clay Nanocomposites: Influence of the Morphology and Polymer/Clay Interactions. *J. Polym. Sci., Part B: Polym. Phys.* **2005,** *43* (2), 205-214.

98. Triantafyllidis, K. S.; LeBaron, P. C.; Park, I.; Pinnavaia, T. J. Epoxy-Clay Fabric Film Composites with Unprecedented Oxygen-Barrier Properties. *Chem. Mater.* **2006,** *18* (18), 4393-4398.

99. Iler, R. Multilayers of Colloidal Particles. *J. Colloid Interface Sci.* **1966,** *21* (6), 569-594.

100. Decher, G.; Hong, J. D.; Schmitt, J. Buildup of Ultrathin Multilayer Films by a Self-Assembly Process: iii. Consecutively Alternating Adsorption of Anionic and Cationic Polyelectrolytes on Charged Surfaces. *Thin Solid Films* **1992,** *210–211, Part 2* (0), 831-835.

101. Borges, J.; Mano, J. F. Molecular Interactions Driving the Layer-by-Layer Assembly of Multilayers. *Chem. Rev.* **2014,** *114* (18), 8883-8942.

102. Stevens, B.; Dessiatova, E.; Hagen, D. A.; Todd, A. D.; Bielawski, C. W.; Grunlan, J. C. Low-Temperature Thermal Reduction of Graphene Oxide Nanobrick Walls: Unique Combination of High Gas Barrier and Low Resistivity in Fully Organic Polyelectrolyte Multilayer Thin Films. *ACS Appl. Mater. Interfaces* **2014,** *6* (13), 9942-9945.

103. Gribova, V.; Auzely-Velty, R.; Picart, C. Polyelectrolyte Multilayer Assemblies on Materials Surfaces: From Cell Adhesion to Tissue Engineering. *Chem. Mater.* **2011,** *24* (5), 854-869.

104. Tang, Z.; Wang, Y.; Podsiadlo, P.; Kotov, N. A. Biomedical Applications of Layer-by-Layer Assembly: From Biomimetics to Tissue Engineering. *Adv. Mater.* **2006,** *18* (24), 3203-3224.

105. Lee, S. W.; Kim, B.-S.; Chen, S.; Shao-Horn, Y.; Hammond, P. T. Layer-by-Layer Assembly of All Carbon Nanotube Ultrathin Films for Electrochemical Applications. *J. Am. Chem. Soc.* **2008,** *131* (2), 671-679.

106. Borges, J.; Rodrigues, L. C.; Reis, R. L.; Mano, J. F. Layer-by-Layer Assembly of Light-Responsive Polymeric Multilayer Systems. *Adv. Funct. Mater.* **2014,** *24* (36), 5624-5648.

107. Zhou, J.; Pishko, M. V.; Lutkenhaus, J. L. Thermoresponsive Layer-by-Layer Assemblies for Nanoparticle-Based Drug Delivery. *Langmuir* **2014,** *30* (20), 5903-5910.

108. Quadir, M. A.; Morton, S. W.; Deng, Z. J.; Shopsowitz, K. E.; Murphy, R. P.; Epps, T. H.; Hammond, P. T. PEG–Polypeptide Block Copolymers as pH-Responsive Endosome-Solubilizing Drug Nanocarriers. *Mol. Pharmaceutics* **2014,** *11* (7), 2420-2430.

109. Yang, Y.-H.; Malek, F. A.; Grunlan, J. C. Influence of Deposition Time on Layer-by-Layer Growth of Clay-Based Thin Films. *Ind. Eng. Chem. Res.* **2010,** *49* (18), 8501-8509.

110. Xiang, F.; Tzeng, P.; Sawyer, J. S.; Regev, O.; Grunlan, J. C. Improving the Gas Barrier Property of Clay–Polymer Multilayer Thin Films Using Shorter Deposition Times. *ACS Appl. Mater. Interfaces* **2014**, in press.

111. Mermut, O.; Barrett, C. J. Effects of Charge Density and Counterions on the Assembly of Polyelectrolyte Multilayers. *The Journal of Physical Chemistry B* **2003,** *107* (11), 2525-2530.

112. Lvov, Y.; Decher, G.; Moehwald, H. Assembly, Structural Characterization, and Thermal Behavior of Layer-by-Layer Deposited Ultrathin Films of Poly(vinyl sulfate) and Poly(allylamine). *Langmuir* **1993,** *9* (2), 481-486.

113. Lvov, Y.; Ariga, K.; Ichinose, I.; Kunitake, T. Assembly of Multicomponent Protein Films by Means of Electrostatic Layer-by-Layer Adsorption. *J. Am. Chem. Soc.* **1995,** *117* (22), 6117-6123.

114. Mateos, A. J.; Cain, A. A.; Grunlan, J. C. Large-Scale Continuous Immersion System for Layer-by-Layer Deposition of Flame Retardant and Conductive Nanocoatings on Fabric. *Ind. Eng. Chem. Res.* **2014,** *53* (15), 6409-6416.

115. Izquierdo, A.; Ono, S. S.; Voegel, J. C.; Schaaf, P.; Decher, G. Dipping versus Spraying: Exploring the Deposition Conditions for Speeding Up Layer-by-Layer Assembly. *Langmuir* **2005,** *21* (16), 7558-7567.

116. Carosio, F.; Di Blasio, A.; Cuttica, F.; Alongi, J.; Frache, A.; Malucelli, G. Flame Retardancy of Polyester Fabrics Treated by Spray-Assisted Layer-by-Layer Silica Architectures. *Ind. Eng. Chem. Res.* **2013,** *52* (28), 9544-9550.

117. Saetia, K.; Schnorr, J. M.; Mannarino, M. M.; Kim, S. Y.; Rutledge, G. C.; Swager, T. M.; Hammond, P. T. Spray-Layer-by-Layer Carbon Nanotube/Electrospun Fiber Electrodes for Flexible Chemiresistive Sensor Applications. *Adv. Funct. Mater.* **2014,** *24* (4), 492-502.

118. Decher, G. Layer-by-Layer Assembly (Putting Molecules to Work). In *Multilayer Thin Films*; Wiley-VCH Verlag GmbH & Co. KGaA, 2012, pp 1-21.

119. Habazaki, H.; Kimura, T.; Aoki, Y.; Tsuji, E.; Yano, T. Highly Enhanced Corrosion Resistance of Stainless Steel by Sol-Gel Layer-by-Layer Aluminosilicate Thin Coatings. *J. Electrochem. Soc.* **2014,** *161* (1), C57-C61.

120. Krogman, K. C.; Lowery, J. L.; Zacharia, N. S.; Rutledge, G. C.; Hammond, P. T. Spraying Asymmetry into Functional Membranes Layer-by-Layer. *Nat Mater* **2009,** *8* (6), 512-518.

121. Choi, I.; Suntivich, R.; Plamper, F. A.; Synatschke, C. V.; Müller, A. H. E.; Tsukruk, V. V. pH-Controlled Exponential and Linear Growing Modes of Layer-by-Layer Assemblies of Star Polyelectrolytes. *J. Am. Chem. Soc.* **2011,** *133* (24), 9592-9606.

122. Silva, J. M.; Georgi, N.; Costa, R.; Sher, P.; Reis, R. L.; Van Blitterswijk, C. A.; Karperien, M.; Mano, J. F. Nanostructured 3D Constructs Based on Chitosan and Chondroitin Sulphate Multilayers for Cartilage Tissue Engineering. *PloS one* **2013,** *8* (2), e55451.

123. Sher, P.; Custódio, C. A.; Mano, J. Layer-by-Layer Technique for Producing Porous Nanostructured 3D Constructs Using Moldable Freeform Assembly of Spherical Templates. *Small* **2010,** *6* (23), 2644-2648.

124. Yu, B.; Liu, X. M.; Cong, H. L.; Wang, Z. H.; Tang, J. G. Fabrication of Stable Ultrathin Transparent Conductive Graphene Micropatterns Using Layer by Layer Self-Assembly. *Sci. Adv. Mater.* **2013,** *5* (11), 1533-1538.

125. Akagi, T.; Fujiwara, T.; Akashi, M. Inkjet Printing of Layer-by-Layer Assembled Poly(lactide) Stereocomplex with Encapsulated Proteins. *Langmuir* **2014,** *30* (6), 1669-1676.

126. Ariga, K.; Nakanishi, T.; Michinobu, T. Immobilization of Biomaterials to Nano-Assembled Films (Self-Assembled Monolayers, Langmuir-Blodgett Films, and Layer-by-Layer Assemblies) and Their Related Functions. *Journal of Nanoscience and Nanotechnology* **2006,** *6* (8), 2278-2301.

127. Arunvisut, S.; Phummanee, S.; Somwangthanaroj, A. Effect of Clay on Mechanical and Gas Barrier Properties of Blown Film Ldpe/Clay Nanocomposites. *J. Appl. Polym. Sci.* **2007,** *106* (4), 2210-2217.

128. Kim, H.; Miura, Y.; Macosko, C. W. Graphene/Polyurethane Nanocomposites for Improved Gas Barrier and Electrical Conductivity. *Chem. Mater.* **2010,** *22* (11), 3441-3450.

129. Vladimirov, V.; Betchev, C.; Vassiliou, A.; Papageorgiou, G.; Bikiaris, D. Dynamic Mechanical and Morphological Studies of Isotactic Polypropylene/Fumed Silica Nanocomposites with Enhanced Gas Barrier Properties. *Compos. Sci. Technol.* **2006,** *66* (15), 2935-2944.

130. Lee, J.-H.; Jung, D.; Hong, C.-E.; Rhee, K. Y.; Advani, S. G. Properties of Polyethylene-Layered Silicate Nanocomposites Prepared by Melt Intercalation with a Pp-G-Ma Compatibilizer. *Compos. Sci. Technol.* **2005,** *65* (13), 1996-2002.

131. Najafi, N.; Heuzey, M.; Carreau, P. Polylactide (PLA)-Clay Nanocomposites Prepared by Melt Compounding in the Presence of a Chain Extender. *Compos. Sci. Technol.* **2012,** *72* (5), 608-615.

132. Kotov, N. A.; Magonov, S.; Tropsha, E. Layer-by-Layer Self-Assembly of Alumosilicate−Polyelectrolyte Composites: Mechanism of Deposition, Crack Resistance, and Perspectives for Novel Membrane Materials. *Chem. Mater.* **1998,** *10* (3), 886-895.

133. Jang, W.-S.; Rawson, I.; Grunlan, J. C. Layer-by-Layer Assembly of Thin Film Oxygen Barrier. *Thin Solid Films* **2008,** *516* (15), 4819-4825.

134. Kim, D.; Tzeng, P.; Barnett, K. J.; Yang, Y.-H.; Wilhite, B. A.; Grunlan, J. C. Highly Size-Selective Ionically Crosslinked Multilayer Polymer Films for Light Gas Separation. *Adv. Mater.* **2014,** *26* (5), 746-751.

135. Priolo, M. A.; Holder, K. M.; Greenlee, S. M.; Grunlan, J. C. Transparency, Gas Barrier, and Moisture Resistance of Large-Aspect-Ratio Vermiculite Nanobrick Wall Thin Films. *ACS Appl. Mater. Interfaces* **2012,** *4* (10), 5529-5533.

136. Carosio, F.; Colonna, S.; Fina, A.; Rydzek, G.; Hemmerlé, J.; Jierry, L.; Schaaf, P.; Boulmedais, F. Efficient Gas and Water Vapor Barrier Properties of Thin Poly(lactic acid) Packaging Films: Functionalization with Moisture Resistant Nafion and Clay Multilayers. *Chem. Mater.* **2014,** *26* (19), 5459-5466.

137. Porcel, C.; Lavalle, P.; Ball, V.; Decher, G.; Senger, B.; Voegel, J.-C.; Schaaf, P. From Exponential to Linear Growth in Polyelectrolyte Multilayers. *Langmuir* **2006,** *22* (9), 4376-4383.

138. Jang, W.-S.; Grunlan, J. C. Robotic Dipping System for Layer-by-Layer Assembly of Multifunctional Thin Films. *Rev. Sci. Instrum.* **2005,** *76* (10).

139. McAloney, R. A.; Goh, M. C. In Situ Investigations of Polyelectrolyte Film Formation by Second Harmonic Generation. *The Journal of Physical Chemistry B* **1999,** *103* (49), 10729-10732.

140. Krebs, F. C. Fabrication and Processing of Polymer Solar Cells: A Review of Printing and Coating Techniques. *Sol. Energy Mater. Sol. Cells* **2009,** *93* (4), 394-412.

141. Hagen, D. A.; Box, C.; Greenlee, S.; Xiang, F.; Regev, O.; Grunlan, J. C. High Gas Barrier Imparted by Similarly Charged Multilayers in Nanobrick Wall Thin Films. *RSC Adv.* **2014,** *4* (35), 18354-18359.

142. Kim, Y. S.; Harris, R.; Davis, R. Innovative Approach to Rapid Growth of Highly Clay-Filled Coatings on Porous Polyurethane Foam. *ACS Macro Lett.* **2012,** *1* (7), 820-824.

143. Ploehn, H. J.; Liu, C. Y. quantitative Analysis of Montmorillonite Platelet Size by Atomic Force Microscopy. *Ind. Eng. Chem. Res.* **2006,** *45* (21), 7025-7034.

144. Tran, N. H.; Dennis, G. R.; Milev, A. S.; Kannangara, G. S. K.; Wilson, M. A.; Lamb, R. N. Interactions of Sodium Montmorillonite with Poly(acrylic acid). *J. Colloid Interface Sci.* **2005,** *290* (2), 392-396.

145. Billingham, J.; Breen, C.; Yarwood, J. Adsorption of Polyamine, Polyacrylic Acid and Polyethylene Glycol on Montmorillonite: An In Situ Study Using ATR-FTIR. *Vib. Spectrosc* **1997,** *14* (1), 19-34.

146. Richert, L.; Lavalle, P.; Payan, E.; Shu, X. Z.; Prestwich, G. D.; Stoltz, J. F.; Schaaf, P.; Voegel, J. C.; Picart, C. Layer by Layer Buildup of Polysaccharide Films: Physical Chemistry and Cellular Adhesion Aspects. *Langmuir* **2004,** *20* (2), 448-458.

147. Picart, C.; Lavalle, P.; Hubert, P.; Cuisinier, F. J. G.; Decher, G.; Schaaf, P.; Voegel, J. C. Buildup Mechanism for Poly(l-lysine)/Hyaluronic Acid Films onto a Solid Surface. *Langmuir* **2001,** *17* (23), 7414-7424.

148. Eaton, P. W. P. *Atomic Force Microscopy*; Oxford Univ. Press: Oxford 2010.

149. Shiratori, S. S.; Rubner, M. F. pH-Dependent Thickness Behavior of Sequentially Adsorbed Layers of Weak Polyelectrolytes. *Macromolecules* **2000,** *33* (11), 4213-4219.

150. Yoo, D.; Shiratori, S. S.; Rubner, M. F. Controlling Bilayer Composition and Surface Wettability of Sequentially Adsorbed Multilayers of Weak Polyelectrolytes. *Macromolecules* **1998,** *31* (13), 4309-4318.

151. Peng, C.; Thio, Y. S.; Gerhardt, R. A.; Ambaye, H.; Lauter, V. pH-Promoted Exponential Layer-by-Layer Assembly of Bicomponent Polyelectrolyte/Nanoparticle Multilayers. *Chem. Mater.* **2011,** *23* (20), 4548-4556.

152. Choi, J.; Rubner, M. F. Influence of the Degree of Ionization on Weak Polyelectrolyte Multilayer Assembly. *Macromolecules* **2004,** *38* (1), 116-124.

153. Mészáros, R.; Thompson, L.; Bos, M.; de Groot, P. Adsorption and Electrokinetic Properties of Polyethylenimine on Silica Surfaces. *Langmuir* **2002,** *18* (16), 6164-6169.

154. Tombácz, E.; Szekeres, M. Colloidal Behavior of Aqueous Montmorillonite Suspensions: The Specific Role of Ph in the Presence of Indifferent Electrolytes. *Appl. Clay Sci.* **2004,** *27* (1–2), 75-94.

155. Podsiadlo, P.; Kaushik, A. K.; Arruda, E. M.; Waas, A. M.; Shim, B. S.; Xu, J. D.; Nandivada, H.; Pumplin, B. G.; Lahann, J.; Ramamoorthy, A.; Kotov, N. A. Ultrastrong and Stiff Layered Polymer Nanocomposites. *Science* **2007,** *318* (5847), 80-83.

156. Fornes, T. D.; Yoon, P. J.; Keskkula, H.; Paul, D. R. Nylon 6 Nanocomposites: The Effect of Matrix Molecular Weight. *Polymer* **2001,** *42* (25), 09929-09940.

157. Priolo, M. A.; Holder, K. M.; Greenlee, S. M.; Stevens, B. E.; Grunlan, J. C. Precisely Tuning the Clay Spacing in Nanobrick Wall Gas Barrier Thin Films. *Chem. Mater.* **2013,** *25* (9), 1649-1655.